MSc in Geographical Information Science

Spatial Patterns of Volcanic Ash Advisories: How the Relationship Between Eruption Characteristics, Ash Cloud Extent and Airport Location Drive Global Aviation Disruption

Frederick Gower Isaac

I declare that this dissertation represents my own work, and that where the work of others has been used it has been duly accredited. I further declare that the length of the components of this dissertation is 4985 words for the Research Paper and 5762 words for the Technical Report

I agree that this dissertation and associated electronic documents, web pages, data, files and computer programs can be retained by the University. YES

I agree that, with the permission of my supervisor(s) or the Programme Director, these materials be made available for the purposes of preparing a publication. YES

I agree that, with the permission of my supervisor(s) or the Programme Director, these materials can be used within the University of Edinburgh for continued research. YES

FREDERICK GOWER ISAAC

06/08/2025

Acknowledgments

I would like to express my gratitude to my supervisor, Dr. Anthony Newton for his guidance, and support throughout this project. In addition, I am thankful to Dr. Samantha Engwell and Dr. John Stevenson from the British Geological Survey for providing me with both the project framework and data, without which this study would not have been possible. Finally, thanks to my family and friends for their support and motivation during the project.

PART I:

Research Paper

Abstract

Volcanic ash clouds generated by explosive eruptions pose a major risk to global aviation, capable of disrupting flight operations globally. These fine particles, though not immediately life-threatening, can damage aircraft engines, reduce visibility and force widespread airspace closures. To mitigate these hazards, Volcanic Ash Advisory Centres (VAACs) provide global monitoring and issue warnings Volcanic Ash Advisories (VAAs) based on satellite observations and dispersion models. This study aims to address the current lack of understanding regarding the spatial extent of volcanic ash clouds and their implication for global aviation disruption, by analysing VAAs issued between 2020 and 2025. Here we show that the severity of disruption is not always determined by ash duration or extent, but rather by the location of impacted airports, particularly those with high passenger throughput. The findings reveal that stratovolcanoes with andesitic compositions are the most frequent sources of high-altitude plumes, consistent with eruption databases based on ash deposits. Importantly there are other factors which affect the level of disruption such as time of year of advisory or the availability of alternative transport. By identifying regions and airspaces more frequently affected by ash, this research can inform flight planning and aviation risk management strategies, especially for vulnerable island nations and major transport hubs.

Keywords: Volcanic Ash Clouds Extent, Volcanic Ash Advisories, Flight Disruption

1. Introduction

Volcanic eruptions generate a number of hazards, including pyroclastic flows, lahars and tephra. Tephra encompasses all volcanic material ejected during an eruption, ranging from fine ash to large volcanic bombs. This thesis focuses specifically on volcanic ash, the finest component of tephra, consisting of particles typically smaller than 2 mm in diameter, formed by the explosive fragmentation of magma (Paredes-Mariño et al., 2022). These fragments result from magma breaking apart, as gas bubbles transition into a continuous gas phase containing suspended molten particles (Zimanowski et al., 2003).

Although volcanic ash is not immediately life-threatening, it poses a significant risk to aviation as it can be transported over vast distances by prevailing winds (Wilson et al., 2012). Ash ingestion can cause jet engine failure, as engines operate at temperatures exceeding 800 °C. At these temperatures, ash becomes sticky when heated through its glass transition range, allowing it to melt and adhere to engine components. This can clog fuel nozzles and damage turbine blades, posing a serious risk to engine performance (Prata and Rose, 2015). In addition, due to the abrasive nature of volcanic ash, prolonged exposure can damage the aircraft's cockpit windows, reducing visibility and compromising flight safety (Drexler et al., 2011). Consequently, ash clouds frequently result in widespread flight cancellations and severe operational disruption (Reichardt et al., 2018).

Plume height and ash cloud extent measurement is critical for impact forecasting, dispersion modelling, and aviation risk management (Cronin, 2013; Horváth et al., 2021). To mitigate these risks, the International Airways Volcano Watch (IAVW) established nine Volcanic Ash Advisory Centres (VAACs) worldwide in the 1990s (Figure 1). These centres are responsible for monitoring volcanic activity and tasked with issuing ash hazard information to pilots, air traffic controllers and metrological watch offices. This hazard information is communicated in the form of a volcanic ash advisory (VAA) which provides graphical projections of ash cloud dispersion based on numerical atmospheric models informed by eruption observations (Watkin, 2003). Although VAAs do not legally close airspace, they are typically interpreted by aviation authorities and airlines as grounds to suspend flights in affected areas, effectively resulting in a no-fly zone wherever ash is present (Civil Aviation Authority, 2017; Clarkson et al., 2016).

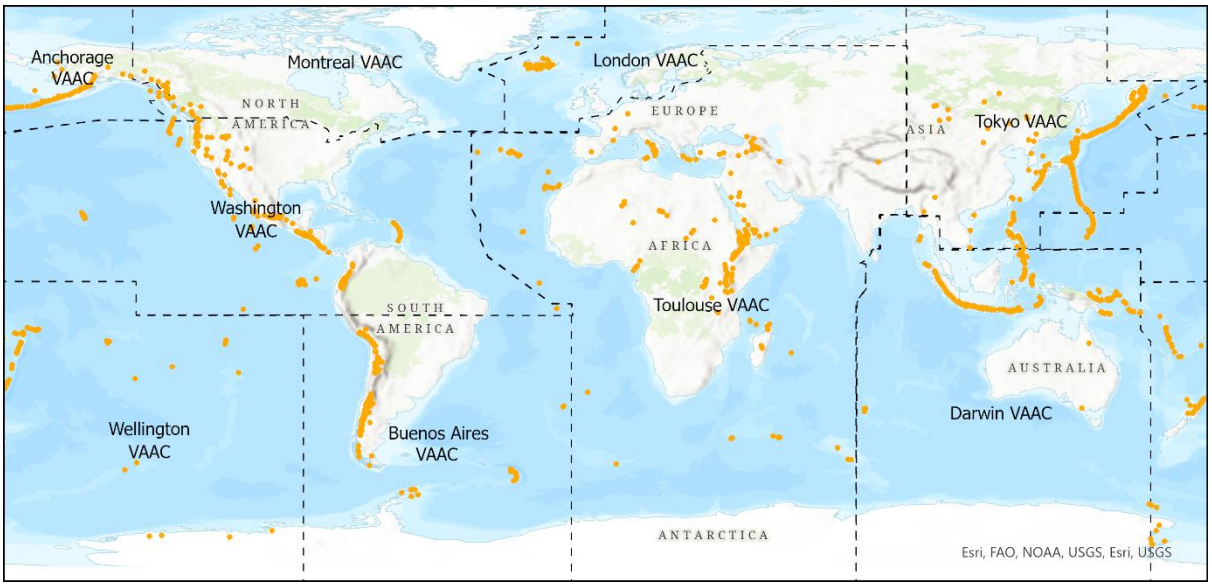

Figure 1: Map of the VAAC area of responsibilities and their volcanoes within them (Smithsonian Institution, 2025).

Table 1: Number of Volcanoes in each VAAC AoR (area of responsibility).

VAAC	No of Volcanoes
Tokyo	267
Washington	247
Toulouse	210
Darwin	184
Buenos Aires	139
Wellington	92
Anchorage	82
London	37
Montreal	22

The 2010 Eyjafjallajökull eruption underscored the vulnerability of global aviation to volcanic eruptions causing over 100,000 flights cancellations, mostly between Europe and North America, and incurring estimated economic losses of $5 billion (Bye, 2014). The economic consequences for business are not limited to a loss in airline ticket sales, but also the movement of goods. More than one fifth of the economy of Kenya relies on exporting flowers to Europe by air; the 2010 volcano eruption caused 1 million roses to be destroyed and delayed vital bone marrow transport from the US to Europe (Alexander, 2013). Whilst such

high profile events attract global headlines, smaller eruptions routinely disrupt air traffic and can cause economic losses particularly in isolated regions that have few airports and are reliant on tourism (Delbrel et al., 2025; Picquout et al., 2013).

Advances in satellite observation, such as the launch of the GOES-16 satellite in 2016, have significantly improved refresh rates from around 15 minutes to 1 minute; and doubling the spatial resolution has significantly enhanced ash detection capabilities compared to those of the Meteosat Second Generation satellites during the 2010 Eyjafjallajökull eruption (Mastin et al., 2022; Prata and Prata, 2012) (Technical Report, 2.1). These enhanced capabilities have enabled integration of thermal infrared brightness temperature difference techniques, allowing more accurate differentiation of volcanic ash from other atmospheric constituents. Modern tools such as the Volcanic Clouds Analysis Tool also provide automatic detection of SO_2 emissions and rising plumes, improving the timeliness and reliability of early warnings (De Angelis et al., 2012).

Technological improvements have contributed to an observed increase in VAAs issued worldwide, likely reflecting improved observational capabilities rather than a true increase in eruptive activity (Engwell et al., 2021). Despite this, critical gaps remain in understanding ash cloud distribution, particularly their relationship with volcanic characteristics, spatial distribution patterns and the number of people affected.

Current research, including Engwell et al. (2021) has identified regions of increased volcanic activity. However, such analyses often overlook the size and extent of volcanic ash clouds, which are critical for assessing aviation disruption. For aviation, the primary hazard lies not in the volcanic eruption itself, but in the wide dispersal of ash, which can affect airspace far from the eruption source. Identifying regions and volcanoes that produce the largest ash clouds is essential, as previous studies highlight the importance of pinpointing hotspots and enhancing monitoring there (Bossi et al., 2024).

To date, no study has investigated the spatial extent of volcanic ash clouds. While earlier efforts, such as Guffanti et al. (2009), catalogued airports affected by ash disruptions, they did not account for passenger volumes. Without this contextual data, quantifying the operational and economic consequences of volcanic ash events on global air travel remains challenging.

This study addresses these gaps by analysing the spatial distribution of VAAs, focusing on global patterns in ash cloud distribution and their implications for air travel.

The purpose of this thesis is to present global patterns in volcanic ash cloud distribution and highlight gaps in the current understanding of ash clouds extent. It begins with a summary of existing research and aviation risk, followed by a methodology to identify patterns in VAAs and the most affected areas and concludes with key findings and their implications.

Research Aim 1: To analyse volcanic characteristics and their relationship with volcanic ash clouds

Objective

a. To investigate how specific volcanic features influence the characteristics and composition of volcanic ash clouds reported in Volcanic Ash Advisories.

Research Aim 2: To analyse the global distribution of Volcanic Ash Advisories

Objective

a. To identify and characterise global spatial patterns of volcanic ash clouds, including their origin, dispersal areas and frequency, based on VAA records.

Research Aim 3: To assess the impact of volcanic ash clouds on aviation and air travel infrastructure

Objectives

a. To identify airports which face the most disruption from volcanic ash clouds.
b. To understand how external factors influence the severity of disruption caused by ash clouds.

British Geological Survey

This work was conducted in partnership with the British Geological Survey and guided by Dr Samantha Engwell (Volcanologist) and Dr John Stevenson (Software Engineer). They proposed this research as a pilot investigation into the global characteristics, distribution and impacts of volcanic ash clouds.

2. Materials and Methods

2.1 Materials

This study addresses three research aims using spatial data and open-source tools. The analysis integrates data from three primary sources: VAAs, Holocene volcano records, and airport passenger statistics.

Table 2: Datasets (Technical Report, Appendix 2, for a breakdown of the information contained in each dataset).

Dataset	Description	Source
Volcanic Ash Advisories	Nine VAACs issued a total of 57,537 VAAs between 1 January 2020 and 20 June 2025.	British Geological Survey
Volcanoes	1,261 volcanoes that have erupted in the Holocene epoch (~12,000 years).	Smithsonian Institution's Global Volcanism Program (Global Volcanism Program, 2025)
World Airports	A file containing 2,174 airports	World Bank (World Bank, 2019)
Fontanarossa	Monthly Airport Data (2020 – 2025)	Aeroporti (*Airport traffic* data, n.d.)

2.1.1 Data limitation

Despite its utility, the airport dataset presented some inconsistencies. Reported figures did not accurately reflect the actual passenger numbers at the airports when compared to ICAO data. Despite this, a general correlation was still observed. While additional data sources were available, they were either behind paywalls or dispersed across individual airport websites, limiting accessibility. Consequently, although the exact number of affected passengers may not reflect true values, the methodology developed provides a replicable framework for future research using more accurate or comprehensive data.

2.2 Methodology

To address the research questions, the analysis was split into two workflows to examine the volcano - ash cloud relationship and the impact on aviation.

2.2.1 Pre-Processing

Test and exercise data entries were removed, and coordinates were transformed to a 0°–360° longitudinal scale to resolve projection inconsistencies (Technical Report, 2.3.2). A Python script was developed to merge VAA and volcano metadata into a unified GeoJSON file, using the Volcano ID as the unique identifier. This integration allowed plume characteristics to be linked with volcano attributes, improving the understanding of which volcanoes produce the most significant eruptions.

In the VAA, plume heights are reported in flight levels (e.g. FL200 – 20,000 feet). which needed to be converted to height above vent. To enable comparison between volcano characteristics, these values were converted to height above the volcanic vent, accounting for the varying elevations of each vent. The script also calculated ash cloud area to assess whether taller eruptions produced larger ash clouds.

2.2.2 Methodology: Research Question 1 and 2

To group advisories into volcanic events, data was clustered where advisories were issued within 6 hours of the previous one from the same volcano, reflecting the typical VAAC reporting interval when ash is present. Event duration was calculated as the time between the first and last advisory in a group, with 6 additional hours added to represent the duration of the final advisory (Shirato, 2013). This enabled analysis of relationships between event duration and volcano type or eruption style. Ungrouped advisories were assigned a default duration of 6 hours. For each group, upper and lower flight levels were used to calculate the minimum and maximum ash cloud heights.

As each group contained multiple polygons, with each polygon representing a single advisory, the geometries were merged using the Shapely union tool to create a single polygon, showing the outermost extent of each event (Technical Report 2.3.3). This prevented areas from being double-counted where advisories overlapped.

To identify where the VAAs were located, a gridded map using Rasterio was set up. VAAs were rasterised onto the grid, with each grid cell having a value representing the number of times it was affected by volcanic ash, producing a heatmap where higher values indicated greater advisory density. Such maps help geoscientists and policymakers identify spatial risk patterns and support informed mitigation strategies (Scheip and Wegmann, 2021).

Once the data was cleaned and contained with new calculations , it was analysed using R and SQL.

2.2.3 Methodology: Research Question 3

Part two of the analysis followed a similar structure to the first part, but there were several key differences. Since the aim was to identify which airports were most at risk, only VAAs intersecting an airport were included. This approach avoided using volcanic events where only some advisories within an event might affect an airport, which could lead to inaccurate estimates of ash exposure duration. To group that data, the airport was used as the aggregator rather than the volcano as multiple volcanoes can affect the same airport. This allowed for a more accurate understanding of how long ash advisories were present in an airport's airspace**.**

To assess the effect of volcanic activity, potential number of passengers disrupted was estimated. While a small airport might be heavily affected by ash, it may serve few passengers. Therefore, airport annual passenger numbers were used to calculate an average daily passenger count per airport, which was then multiplied by ash exposure duration to understand the potential number of affected passengers.

To evaluate how volcanic ash impacts vary seasonally, monthly passenger data for Fontanarossa Airport was analysed to examine how eruption timing influences the number of people affected. Such detailed monthly passenger data are not available for all airports, so this analysis was limited to locations with reliable records. A linear regression model was applied using monthly passenger count as the outcome variable. The model included two predictors: the number of days of volcanic ash in each month and the month of the year (a categorical variable capturing seasonality). January served as the reference category, allowing the model to account for expected seasonal variations in air travel.

3. Results

3.1 VAAs

Between 1st January 2020 and 20th June 2025, a total of 51,519 VAAs were issued, describing activity at 136 volcanoes worldwide. The Darwin VAAC issued the majority (26,500; 52%), while London VAAC issued the fewest (23). Notably, over 70% of all VAAs originated from only 10 volcanoes, with Sangay (5,478), Reventador (5,295), and Fuego (5,184) accounting for the top three sources of activity. Collectively, these three volcanoes accounted for approximately 30% of all VAAs issued during the study period.

3.2 Volcanic Events

During the same period, 11,548 volcanic events were identified (Figure 2), defined as sequences of VAAs from the same volcano within a 6-hour window. The average event duration was approximately 14 hours, culminating in a combined 21 years of volcanic ash disruption across the period of study. Sangay volcano exhibited the longest lasting activity, with eruptive phases lasting nearly 3 years.

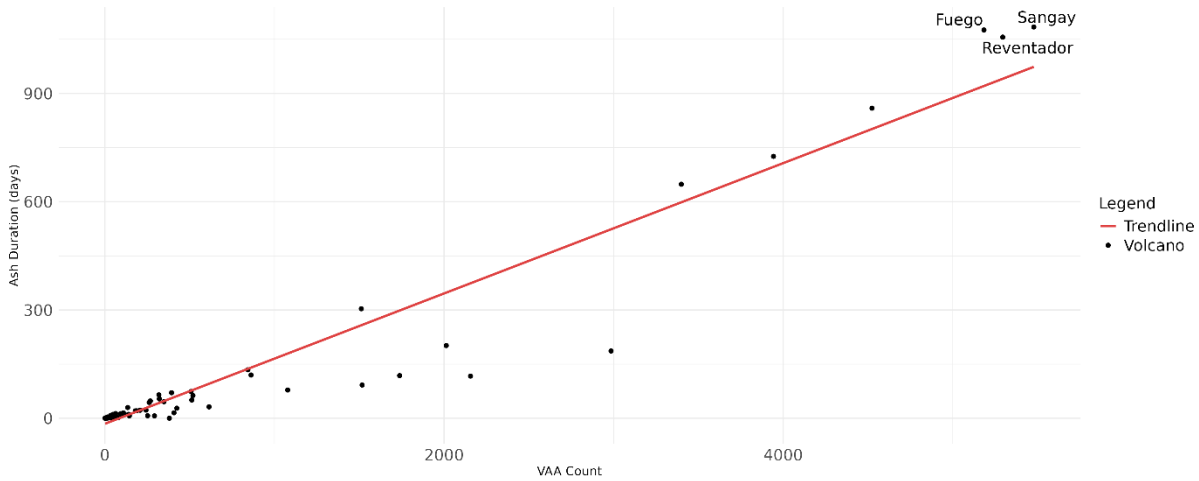

Figure 2: Relationship between the number of volcanic events and the total duration of ash emissions at each active volcano ($r = 0.96$, $p < 0.001$).

3.3 Plume Height Distribution

All recorded plume heights exceeded 12 meters above the volcanic vent. The majority of volcanic events were from stratovolcanoes across all plume heights, with most occurring below 5000 m above the volcanoes summit (Figure 3). In contrast, significantly fewer volcanic events were linked to complex and caldera volcanoes. For plume heights below 4000 m, complex volcanoes were more frequent than caldera volcanoes, whereas between 4000 m and 5000 m caldera volcanoes were more prominent.

Andesitic volcanoes were the most common across all plume heights, particularly over 1000 m above vent. For plume heights under 1,000 m, basalt and dacite volcanoes were also represented, particularly around the 800 m mark. Volcanic events plumes over 10,000 m were fewer and limited to andesitic volcanoes.

Across all plume heights, most volcanic events were within the Washington VAAC AoR (Area of Responsibility), with Buenos Aires, Darwin and Tokyo VAAC also contributing. While this spread reflects the global distribution of volcanoes, Toulouse VAAC has the third largest number (210) of Holocene volcanoes, despite still producing relatively few volcanic events in this study period.

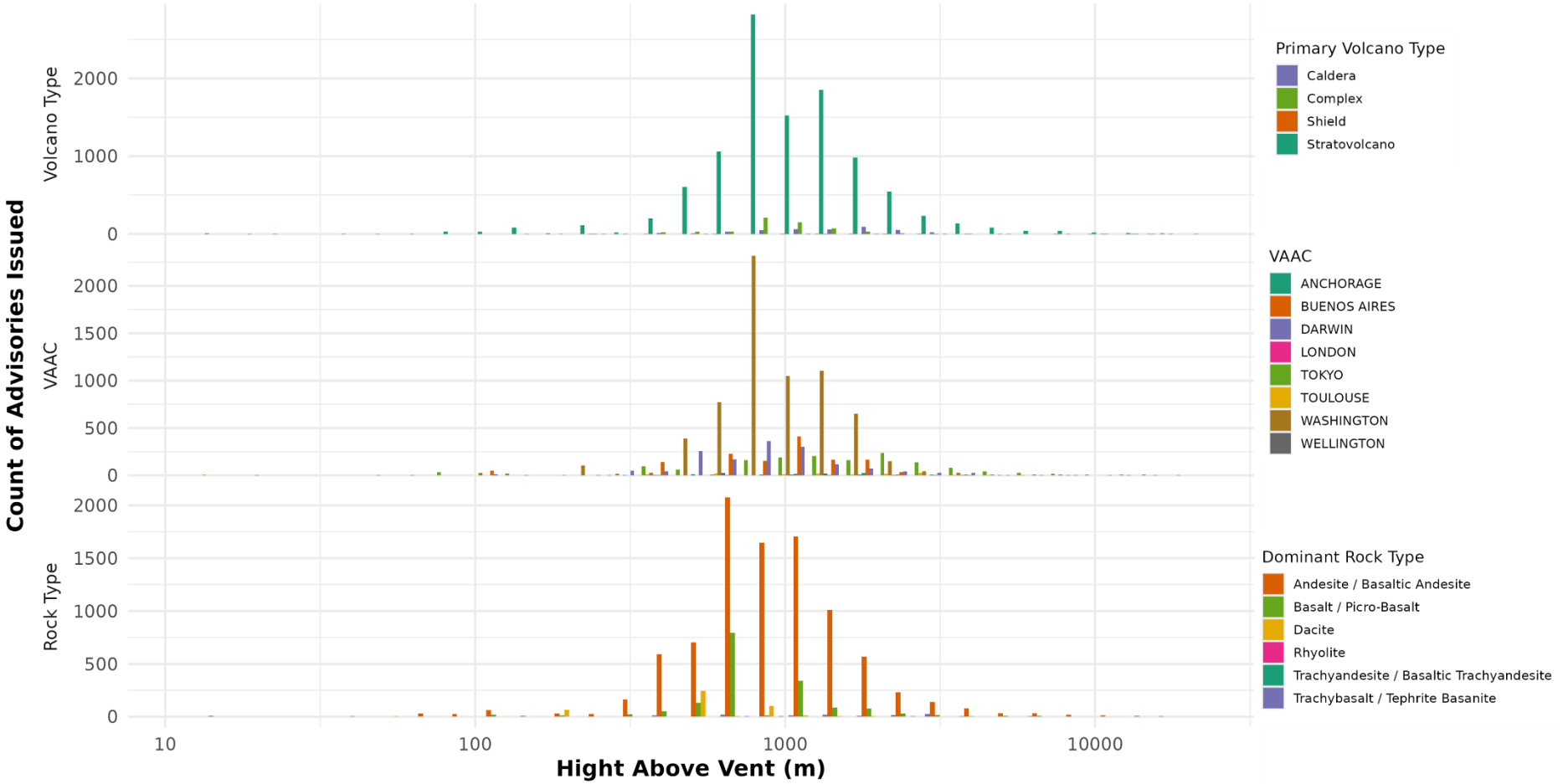

Figure 3: Distribution of Volcanic Events counts relative to volcano summit height across three different groupings: Primary Volcano Type (top), Volcanic Ash Advisory Centre (VAAC, middle), and Dominant Rock Type (bottom). The x-axis represents the volcano's plume height above vent on a logarithmic scale, indicating how Volcanic Event elevation varies with volcano characteristics. Bin count is n = 30.

3.4 Areal Extent Distribution

The observed areas (km²) affected by volcanic ash were extracted for each eruptive event and compared with volcano type, plume characteristics and their VAAC to investigate their relationships.

Stratovolcanoes dominate in terms of the area covered by volcanic ash during an eruptive event and their frequency. Caldera volcanoes were the second most frequent contributor for volcanic events for extents less than 1,000km^2. However, as plume area increased (Figure 4), volcanic events from complex volcanoes were more common. This contrasts with figure 3, where lower plume heights were more common for complex volcanoes and higher plume hights more frequent for caldera volcanoes. This suggests that complex volcanoes produce lower, bigger plumes, whereas caldera volcanoes produce higher but smaller plumes.

Andesitic volcanoes exhibited a wide range of ash extents. However, basalt volcanoes tend to have mid – sized events (800m^2 – 2000m^2), with a few trachybasalt volcanoes exhibiting events exceeding 3000 km².

The majority of Volcanic events were within the Washington VAAC AoR across all plume heights. In comparison, Buenos Aires, Tokyo, and Darwin VAACs had substantially fewer, though still more than the remaining centres. The patterns observed in Figure 3 closely resemble those in Figure 4, suggesting a potential correlation between eruption height and the Volcanic Event Extent.

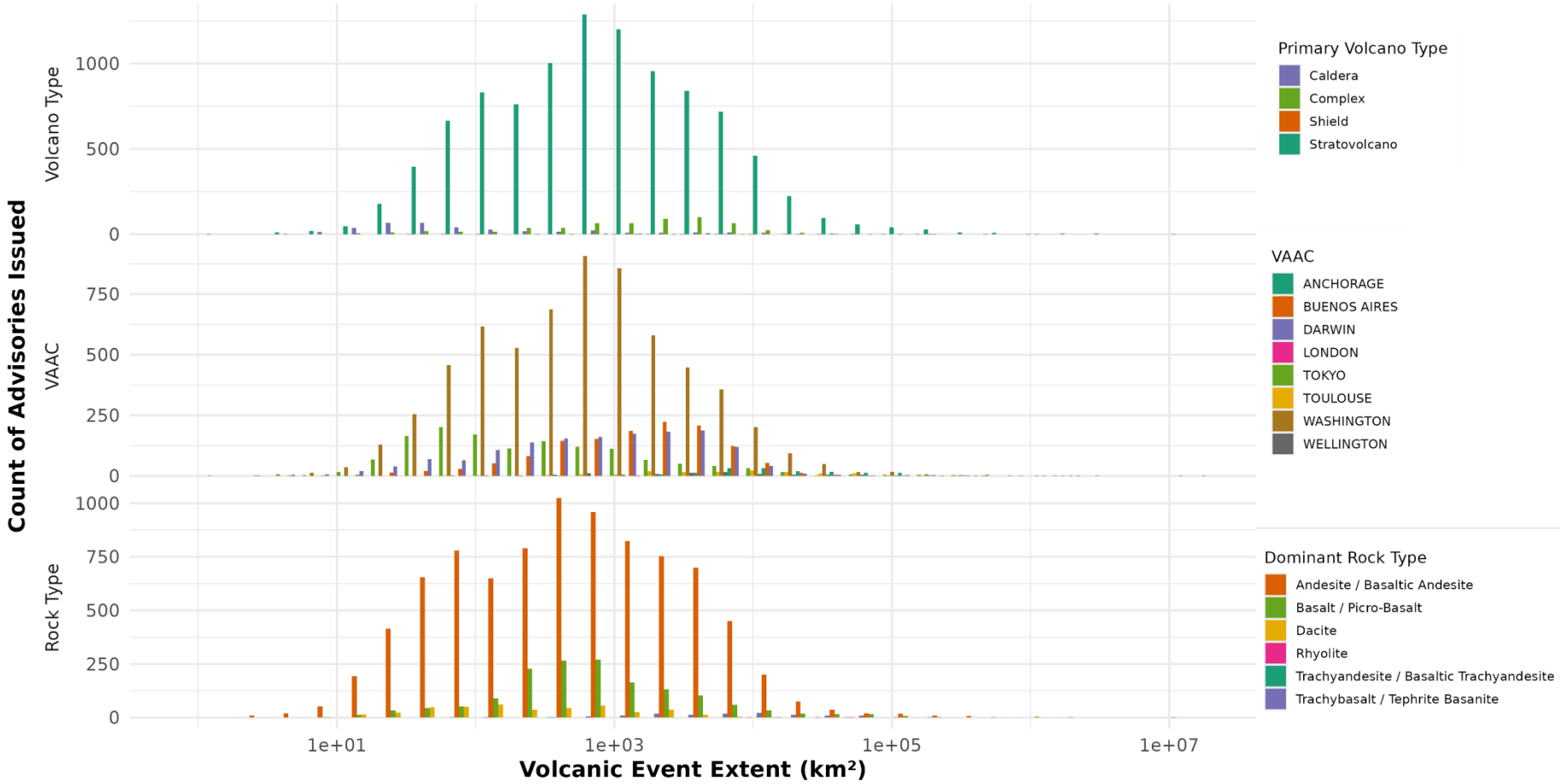

Figure 4: Distribution of Volcanic Events based on the Areal Extent, grouped by Primary Volcano Type (top), VAAC (middle), and Dominant Rock Type (bottom). The x-axis (VAA Area in km²) is shown on a logarithmic scale, revealing patterns in Events frequency relative to the spatial extent of ash dispersion. Bin count is n = 30.

3.5 Areal Extent and Plume Height Relationship

To explore the relationship between eruption plume height and observed area, a correlation analysis was conducted. A positive correlation was found, with a Pearson correlation coefficient of r = 0.304 and a p-value = 1.82×10^{-229}, indicating a statistically significant relationship between larger eruption extents and higher plume heights (Figure 5). While the correlation coefficient suggests only a moderate linear association, the extremely small p-value confirms that the trend is not due to random chance.

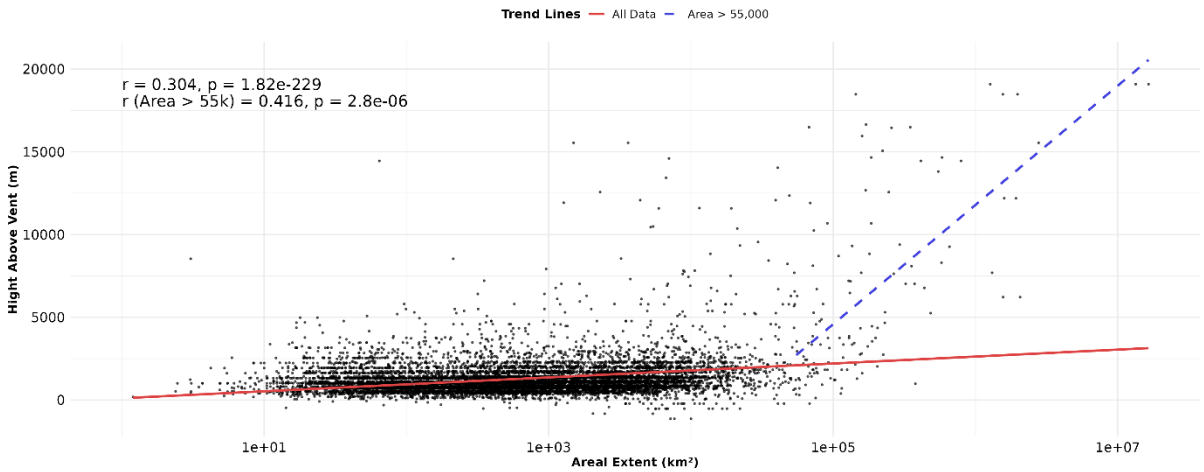

Figure 5: Relationship between the plume height and observed ash extent of a volcanic event. Black dots represent volcanic events.

The trendline shows a positive correlation (Figure 5, Red Line), indicating that advisories with greater areal extents are generally associated with taller plume heights. Interestingly, the pattern appears to shift at larger ash cloud extent. For smaller to mid-sized ash cloud extents, the relationship between area and height remains relatively diffuse, with many data points clustering at lower heights. However, beyond a certain extent threshold (around 10^4 to 10^5 km), eruption height appears to have a stronger influence on area, as evidenced by more frequent high-altitude values and a visibly steeper trend in the upper range (Figure 5, Blue Line).

3.6 Spatial Patterns

Figure 6 illustrates global volcanic ash extent density overlaid with the location of affected airports. High concentrations appear across Southeast Asia, including Indonesia, Papua New Guinea and the Philippines. Similar densities are seen in the northern Pacific, especially Alaska and Russia's Kamchatka Peninsula. In Central and South America, elevated ash cloud densities are associated with volcanic activity in Guatemala, Ecuador, Peru and Chile. Moderate concentration of ash is observed in parts of Europe, particularly southern Italy.

Southeast Asia has significantly the largest area affected (Hunga Tonga eruption), with the advisories spanning vast distances both over oceanic and continental airspaces. However, such eruptions are rare as indicated by their low density. In contrast the northern Pacific and Central and South America, show smaller eruptions but have a larger density reflecting more frequent but less intense activity.

The airports in Figure 6 cluster in southern Europe and Southeast Asia, indicating these are regions of significant population, compared to the North Pacific, where there is little habitation and infrastructure.

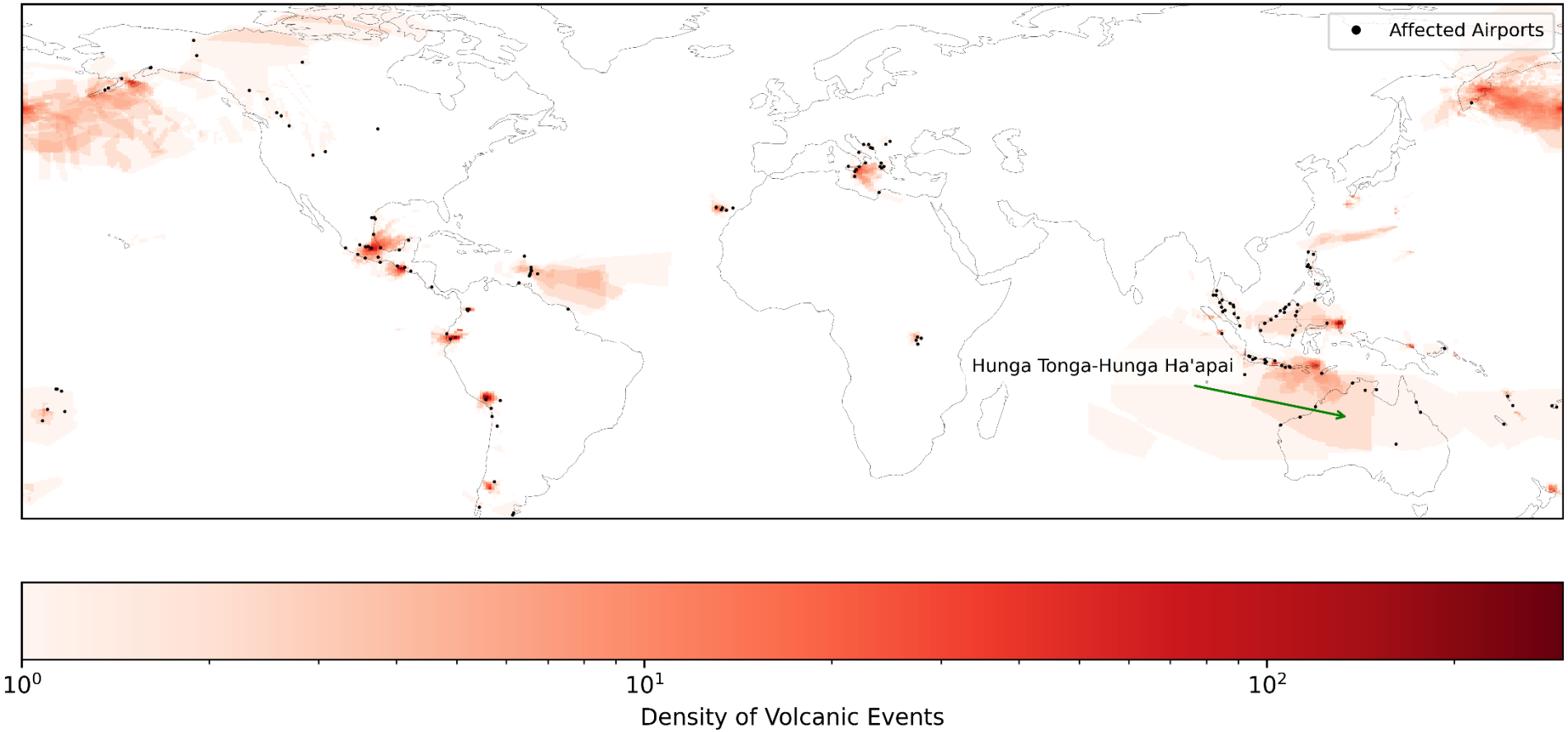

Figure 6: Global density map of volcanic event extents. The colour gradient represents the density of events, with darker reds indicating higher densities. Black dots indicate airports affected by ash clouds during this period.

3.7 Impact on Airports

Figure 7 reinforces the observation that the affected European airports, particularly those within the Toulouse VAAC AoR tend to have some of the highest passenger numbers globally. In addition, it highlights how the impact on volcanic ash on airports varies, with disruption influenced by both passenger volume and ash exposure. For instance, Ngurah Rai Airport (Indonesia) handles over 10 million passengers annually but experiences only a few days of disruption. In contrast, José Joaquín de Olmedo Airport (Ecuador) endured approximately 15 days of disruption yet serves only around 2 million passengers annually. Meanwhile, Fontanarossa Airport (Italy), located just 50 km from Mount Etna, experiences both high passenger volumes and frequent VAAs, making it particularly vulnerable.

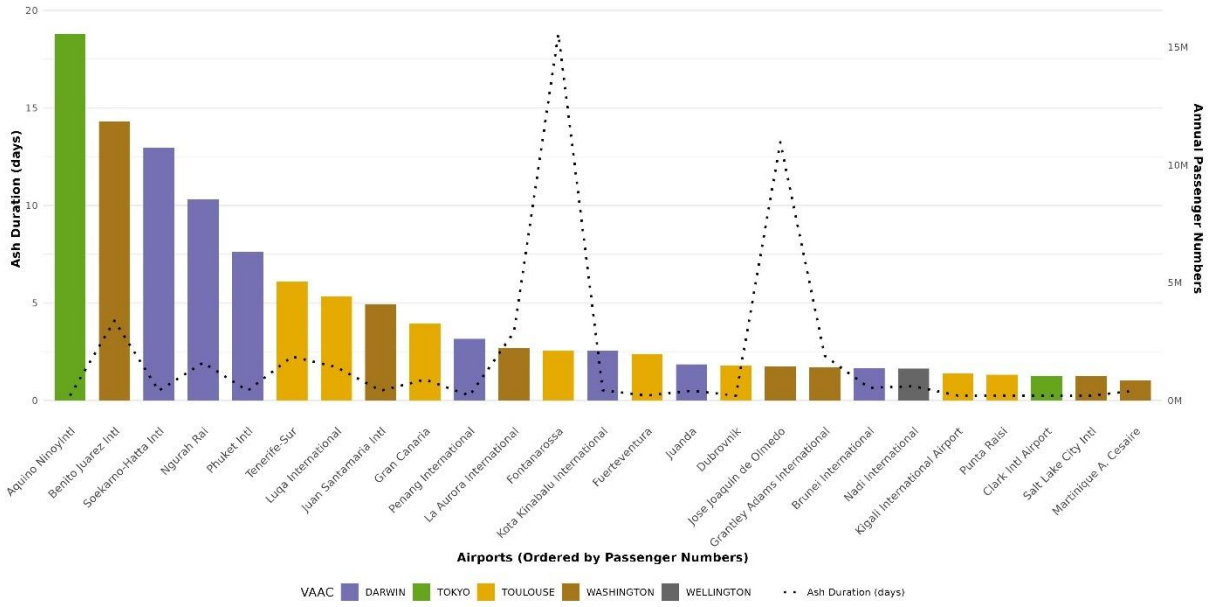

Figure 7: Duration of observed ash in airspace over airports according to polygons within VAA (dotted line) with the average annual passenger numbers (bars) across the 25 busiest airports. Bars are colour coded by the associated Volcanic Ash Advisory Centre (VAAC).

This disparity demonstrates that the impact of volcanic ash on aviation cannot be assessed by ash duration or passenger volume alone; both factors must be considered in tandem.

Disruption levels were assessed by combining volcanic ash exposure and airport activity to estimate operational impact. Benito Juárez experienced the highest level of disruption, with over 100,000 passengers potentially affected, nearly 30,000 more than the next most impacted airport (Figure 8). Other major disruptions were concentrated at airports within the Washington VAAC AoR, including José Joaquín de Olmedo, Benito Juárez, and Grantley Adams, underscoring the underscoring the number of volcanoes within their AoR.

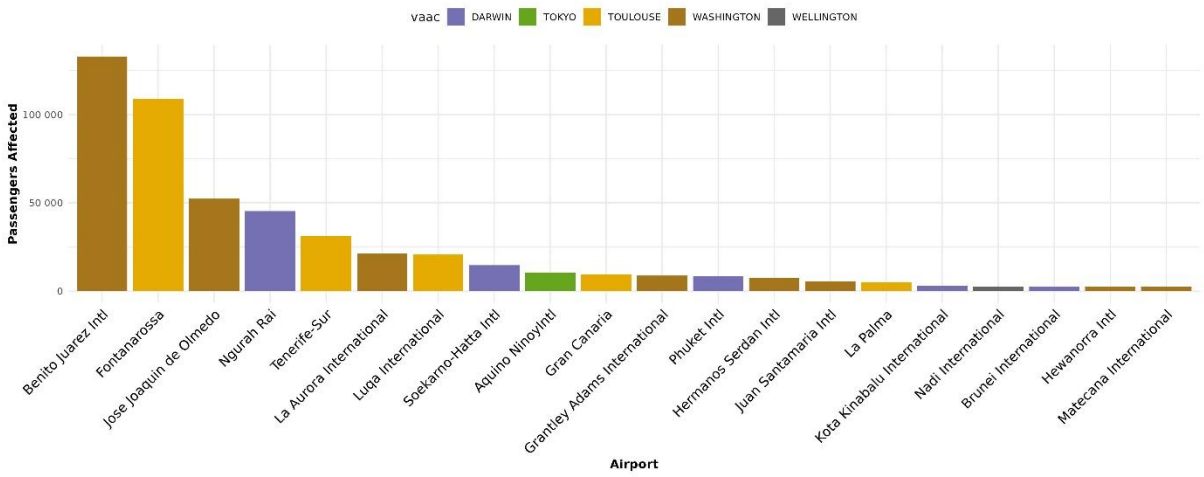

Figure 8: Duration of observed ash in airspace over airports according to polygons within VAA (dotted line) with the average annual passenger numbers (bars) across the 25 busiest airports. Bars are colour coded by the associated VAAC.

Among the top 20 most disrupted airports, those overseen by the Toulouse VAAC stood out, accounting for 25% of the list, despite few Toulouse volcanoes being active in their AoR and relatively few advisories issued (Figures 3 and 4). This suggests that even a small number of advisories can have a disproportionately large impact on passenger traffic if they affect high volume airports such as Fontanarossa Airport (Italy).

While airports within the Tokyo, and Wellington VAAC AoR appeared in the top 20 most affected by volcanic ash, the impact was limited, with lower passenger disruption totals and fewer entries overall.

To assess how volcanic eruption characteristics influence the number of people affected, the relationships between eruption area, duration and affected people were analysed (Figure 9).

There was no significant correlation between the area covered by advisories above airports and the number of people affected (Pearson's r = –0.018, p = 0.817; Fig. 9, top), indicating a negligible and statistically insignificant relationship.

In contrast, a weak but statistically significant positive correlation was found between ash duration above airports and the number of people affected (r = 0.234, p = 0.0026; Fig. 9, bottom) indicating that longer duration may affect more people. Although the strength of this relationship is modest, it suggests that duration may be a more relevant factor than area in determining how many people could be affected.

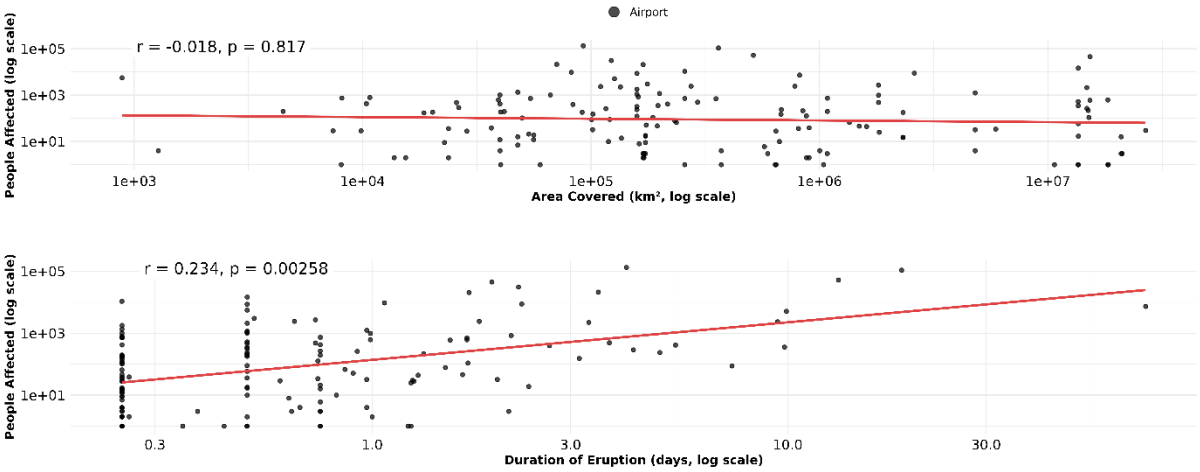

Figure 9: Relationship between airport advisories characteristics and the number of people affected (both axes on a log scale). (Top) Relationship between the area covered by an advisory (in km²) and the number of people affected. (Bottom) Relationship between the duration by an advisory (in days) and the number of people affected.

A regression analysis of passenger traffic and ash duration at Fontanarossa (Figure 10) demonstrated that both volcanic ash from eruptions and seasonal trends significantly ($p < 0.05$) influenced monthly passenger volumes. This is important because it shows that the time of year when an advisory occurs can affect its impact. Specifically, summer months consistently showed higher passenger numbers, while months affected by volcanic eruptions exhibited statistically lower figures.

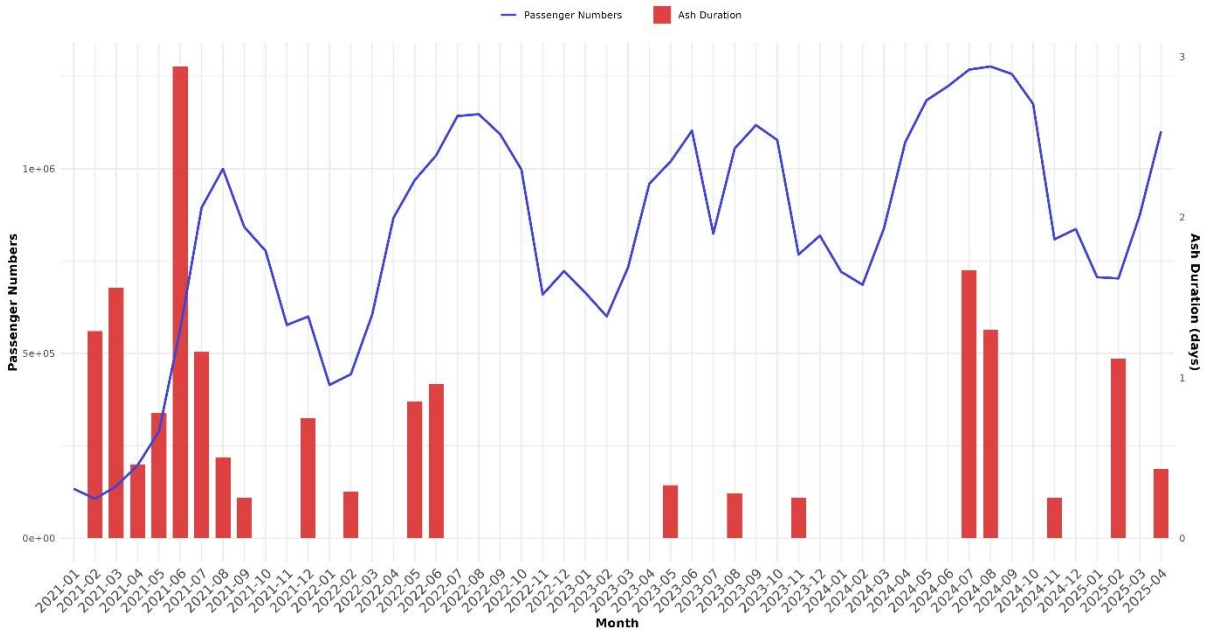

Figure 10: Monthly passenger numbers at Fontanarossa Airport (blue line, left y-axis) and volcanic ash duration from Mt. Etna (red bars, right y-axis), from January 2021 to April 2023 (Airport traffic data, 2025).

In contrast, ash emissions and duration exhibited no seasonal pattern and appeared sporadic throughout the study period. Notable volcanic ash events occurred in March and April 2021, August and September 2021, and August and October 2022. The most severe disruption was observed in July 2021, when ash presence exceeded 2.5 days.

4. Discussion

4.1 Volcano – Ash Cloud relationship

The results show that the majority of the most powerful eruptions, measured by plume height, originate from stratovolcanoes with andesitic compositions (Figures 3&4). This aligns with results from the LaMEVE (Large Magnitude Explosive Volcanic Eruptions) database, where stratovolcanoes (n = 1200) and andesitic compositions (n = 838) are most commonly associated with large magnitude eruptions (VOGRIPA, 2025). The consistency between different data sources, with LaMEVE relying primarily on deposit records (Crosweller et al., 2012) and this study focusing on ash cloud observations, reinforces these findings. However, smaller eruptions are often underrepresented in eruption records due to poor preservation, as ash and other materials erode or are buried quickly. Additionally, researchers may focus on larger eruptions, leading to under-reporting of smaller-scale volcanic activity (Kiyosugi et al., 2015). By including events of all sizes, some with an extent under 10 km^2, this study helps improve understanding of smaller eruptions.

While this work includes smaller eruptions, results from this study are subject to selection bias as the VAA data is collected from satellite observations, affected by satellite overpass frequency, metrological conditions and ash concentration (Engwell et al., 2021). As the dataset spans 2020 – 2025, it benefits from recent advancements in satellite technology, allowing for detection of eruptions that may not produce observable deposits. This creates a bias towards smaller eruptions, which is valuable, as few other resources capture this type of activity. When combined with geological data, the result is a more comprehensive understanding of typical volcanic activity over time.

The results contrast with those of Guffanti et al. (2009) as there is no relationship between area of VAAs and disruption at an airport. However, this discrepancy may be due to methodological differences: while the aforementioned study considers volcanic eruptions in general, my analysis focuses specifically on VAAs that intersect with airports. Despite this, the results highlight that even smaller VAAs can impact airports just as significantly as larger ones.

4.2 VAAs Spatial Pattens

The results show that Washington, Darwin, and Tokyo VAACs recorded the highest number of VAAs, consistent with previous studies (Engwell et al., 2021; Mastin et al., 2022). However, this study observed a higher number of VAAs from the Washington VAAC, as it contained the most frequently active volcanoes: Reventador, Sangay, and Fuego, each of which produced over 1,000 eruptions.

This study builds upon previous research that categorises VAAs by VAAC jurisdiction, country affiliation or volcano (Engwell et al., 2021) by providing additional spatial information locations of the areal extent of volcanic ash clouds.

For example, eruptions from volcanoes like Klyuchevskoy and Bezymianny, which fall under the responsibility of both Anchorage and Tokyo VAACs, are labelled as Russia in the VAA, highlighting that country boundaries and VAAC jurisdictions do not always align. This distinction is crucial when assessing aviation risk, as the critical factor is the location of affected airspace rather than the country of the eruption's origin. By identifying frequently impacted airspace regions, this study offers insights to support better flight planning and improve aircraft avoidance of ash clouds.

4.3 Impact on Airports

The findings show that areas with the longest ash duration are not necessarily those experiencing the greatest disruption. For example, while volcanoes within the Washington, Buenos Aires, and Darwin VAAC AoR record the longest ash durations, it is those within Washington, Toulouse, and Darwin VAAC AoR that face the highest levels of ash duration over airports. This is influenced by the higher density of cities near volcanoes in Europe compared to Buenos Aires, resulting in more airports located close to volcanic hazards and thus greater potential disruption (Meredith et al., 2025).

A similar trend emerges when comparing ash cloud extent and potential airport disruption. Airports like Hermanos Serdán (Mexico) and Fontanarossa (Italy) may experience wide ash spread, but when passenger volume is considered, Benito Juárez International Airport (Mexico City), a major transit hub, shows far more significant disruption, despite having shorter ash durations. This highlights that longer ash exposure does not necessarily equate to greater operational impact, especially if the affected airport serves few passengers.

This aligns with previous research Guffanti et al. (2009), which focused on how frequently volcanic ash has disrupted air travel, rather than the volume of passengers affected. That study identifies Ted Stevens (Alaska) and Tokua Airport (Papua New Guinea) as among the most frequently disrupted airports. However, both are relatively small airports in terms of passenger traffic, so while they may be operationally affected often, the scale of impact on commercial air travel is limited when compared with major international hubs.

4.3.1 Fontanarossa

Monthly passenger data from Fontanarossa Airport, Sicily reveals distinct temporal trends, with peaks during the summer months, likely attributable to the holiday season (Dobruszkes et al., 2022). Statistical analysis confirms that the timing of a volcanic eruptive event significantly influences the number of passengers impacted. This is particularly relevant given Fontanarossa's proximity to Mount Etna, one of Europe's most active volcanoes. However, this seasonal variation is not uniformly observed across all airports. Research indicates that only around 36% of airports worldwide exhibit significant seasonality, with major transit hubs, particularly those serving both business and leisure travel, less affected by fluctuations (Dobruszkes et al., 2019). This suggests that while seasonal patterns are evident at certain regional airports like Fontanarossa, they do not reflect global airport trends.

Island territories are particularly vulnerable to volcanic ash-related disruption due to limited transport alternatives. The 2010 eruption of Mount Merapi exposed this weakness in Indonesia, where the closure of Adisucipto Airport highlighted the limited capacity of the surrounding infrastructure (Technical Report 4.1). Alternative airports like Surakarta and Surabaya required long overland transfers, reducing their effectiveness and revealing the challenges of maintaining connectivity during major volcanic events (Picquout et al., 2013). This highlights how eruptions near airports in such regions can have a greater impact on air travel and the wider economy than airports with more accessible alternatives.

A better understanding of the full impact of volcanic ash and its associated risks to aviation will support scientific development and, in turn, lead to improved operational responses (Witham et al., 2024). With this knowledge, identifying regions with the highest level of disruption is crucial, as highlighted by previous hazard mapping efforts (Bossi et al., 2024), which stresses the importance of enhanced monitoring in hazard hotspots. This alongside the improved detection rate provided by new satellite technologies supports more effective

hazard assessment and early warning systems for both large and small eruptions limiting disruption.

4.3.2 Other considerations

Additional external factors also complicate the assessment of volcanic ash impacts. At Fontanarossa, passenger numbers declined significantly following the COVID-19 pandemic, a trend reflected globally, with some studies reporting reductions of up to 43% compared to 2019 levels (Bielecki et al., 2020). Similarly, a sharp drop in passenger numbers during July 2023 could be attributed to an airport fire (Vagnoni and Amante, 2023) . These external shocks illustrate how factors beyond volcanic activity, such as pandemics and economic downturns can significantly alter the number of people affected by an ash-related disruption. Moreover, it is not only airports with high passenger traffic that are vulnerable to closures; airports with significant cargo flight operations can also experience substantial disruptions and economic impacts due to their critical role in global supply chains (Budd and Ison, 2023; Janić, 2019). For example, Ted Stevens Anchorage Airport was the world's fourth-busiest cargo airport in 2021, serving as a vital hub for goods between Asia and North America (McKinley Research, 2023).

4.4 Limitations

Whilst this work assessed the impact of explosive volcanic events on aviation, there are several key areas of the study which could be improved. Firstly, only those VAAs which included observations of volcanic ash extent were included which means that some events may have been missed. This is a common challenge when working with real world data, which often contains missing data and has data formatting issues (Liu and Panagiotakos, 2022).

In addition, if VAAs were in close proximity to an airport, they could have been considered to be disruptive as the airports data were marked as a point, which has zero area, rather than a polygon showing the extent of the airport, so if an advisory was very close to a point, the ash could lie within the airport perimeter, but not been included in the analysis. In future studies, applying a buffer around each airport point could better represent the true spatial extent of the facility and improve the accuracy of impact assessments.

Lastly, this study used 2019 airport passenger traffic, while the analysis of VAAs covered 2020 to 2025, including the first two years of the COVID-19 pandemic. This temporal mismatch may

overestimate the number of potentially affected passengers, however the global decline in air travel during the pandemic was relatively uniform across airports. As such, the proportional impact between locations is likely preserved, limiting uncertainty in the comparative analysis.

Conclusion

This study analysed global VAAs from January 2020 to May 2025, revealing relationships between eruption characteristics, ash cloud distribution and disruption to aviation. Results confirm that stratovolcanoes with andesitic compositions more commonly produce large-scale ash events, consistent with established eruption databases. Importantly, this research expands existing knowledge by incorporating satellite-derived VAA data, capturing smaller-scale eruptions often omitted from deposit-based records.

Spatial analysis highlighted regional disparities in ash detection and impact, with Washington, Darwin and Tokyo VAACs issuing the most advisories. However, the severity of disruption was not solely determined by ash duration or extent. Airports with high passenger throughput, particularly in remote or island settings with limited alternatives, may experience greater operational impacts.

While limitations in passenger data constrained precise quantification, the study provides a replicable framework for assessing volcanic ash impacts using VAA and aviation data. Future work could incorporate flight path analyses to better understand the effect of ash on aviation, improving disruption forecasting and mitigation strategies. Overall, these findings improve understanding of the spatial extent of volcanic ash and their impact on aviation.

Bibliography

Aeroporti 2030, 2025. Airport traffic data. Aeroporti 2030. URL https://www.aeroporti2030.com/airport-traffic-data/ (accessed 7.30.25).

Alexander, D., 2013. Volcanic ash in the atmosphere and risks for civil aviation: A study in European crisis management. Int J Disaster Risk Sci 4, 9–19. https://doi.org/10.1007/s13753-013-0003-0

Bielecki, M., Patel, D., Hinkelbein, J., Komorowski, M., Kester, J., Ebrahim, S., Rodriguez-Morales, A.J., Memish, Z.A., Schlagenhauf, P., 2020. Reprint of: Air travel and COVID-19 prevention in the pandemic and peri-pandemic period: A narrative review. Travel Medicine and Infectious Disease 38, 101939. https://doi.org/10.1016/j.tmaid.2020.101939

Bossi, G., Cavalli, M., Mantovani, M., Catelan, F.T., Ballaera, A., Ceccotto, F., Marcato, G., Pasuto, A., 2024. Expecting the expected – learning from the past to provide forward scenarios through geomorphic change detection, monitoring and modeling. Geoenviron Disasters 11, 35. https://doi.org/10.1186/s40677-024-00292-7

Budd, L., Ison, S., 2023. Chapter 14 - The impact of COVID-19 on air cargo logistics and supply chains, in: Zhang, J., Hayashi, Y. (Eds.), Transportation Amid Pandemics, World Conference on Transport Research Society. Elsevier, pp. 183–188. https://doi.org/10.1016/B978-0-323-99770-6.00020-X

Civil Aviation Authority, 2017. Guidance regarding flight operations in the vicinity of volcanic ash [WWW Document]. URL https://www.caa.co.uk/safety-initiatives/safety-projects/volcanic-ash/volcanic-ash/ (accessed 8.6.25).

Clarkson, R.J., Majewicz, E.J., Mack, P., 2016. A re-evaluation of the 2010 quantitative understanding of the effects volcanic ash has on gas turbine engines. Proceedings of the Institution of Mechanical Engineers, Part G: Journal of Aerospace Engineering 230, 2274–2291. https://doi.org/10.1177/0954410015623372

Cronin, S.J., 2013. Stratovolcanoes, in: Encyclopedia of Natural Hazards. Springer, Dordrecht, pp. 941–947. https://doi.org/10.1007/978-1-4020-4399-4_333

De Angelis, S., Fee, D., Haney, M., Schneider, D., 2012. Detecting hidden volcanic explosions from Mt. Cleveland Volcano, Alaska with infrasound and ground-coupled airwaves. Geophysical Research Letters 39. https://doi.org/10.1029/2012GL053635

Delbrel, J., Burton, M., Engwell, S., Esse, B., Hayer, C., 2025. An investigation of changes to commercial aircraft flight paths during volcanic eruptions. J Appl. Volcanol. 14, 2. https://doi.org/10.1186/s13617-025-00150-7

Dobruszkes, F., Decroly, J.-M., Suau-Sanchez, P., 2022. The monthly rhythms of aviation: A global analysis of passenger air service seasonality. Transportation Research Interdisciplinary Perspectives 14, 100582. https://doi.org/10.1016/j.trip.2022.100582

Dobruszkes, F., Ramos Pérez, D., Decroly, J.-M., 2019. Reasons for Flying. pp. 23–39. https://doi.org/10.1016/B978-0-12-812857-2.00003-8

Drexler, J.M., Gledhill, A.D., Shinoda, K., Vasiliev, A.L., Reddy, K.M., Sampath, S., Padture, N.P., 2011. Jet Engine Coatings for Resisting Volcanic Ash Damage. Advanced Materials 23, 2419–2424. https://doi.org/10.1002/adma.201004783

Engwell, S., Mastin, L., Tupper, A., Kibler, J., Acethorp, P., Lord, G., Filgueira, R., 2021. Near-real-time volcanic cloud monitoring: insights into global explosive volcanic eruptive activity through analysis of Volcanic Ash Advisories. Bull Volcanol 83, 9. https://doi.org/10.1007/s00445-020-01419-y

Global Volcanism Program, 2025. [Database] Volcanoes of the World (v. 5.3.1; 6 Aug 2025). Distributed by Smithsonian Institution, compiled by Venzke, E. https://doi.org/10.5479/si.GVP.VOTW5-2025.5.3

Guffanti, M., Mayberry, G.C., Casadevall, T.J., Wunderman, R., 2009. Volcanic hazards to airports. Nat Hazards 51, 287–302. https://doi.org/10.1007/s11069-008-9254-2

Horváth, Á., Carr, J.L., Girina, O.A., Wu, D.L., Bril, A.A., Mazurov, A.A., Melnikov, D.V., Hoshyaripour, G.A., Buehler, S.A., 2021. Geometric estimation of volcanic eruption column height from GOES-R near-limb imagery – Part 1: Methodology. Atmospheric Chemistry and Physics 21, 12189–12206. https://doi.org/10.5194/acp-21-12189-2021

Janić, M., 2019. Modeling the resilience of an airline cargo transport network affected by a large scale disruptive event. Transportation Research Part D: Transport and Environment 77, 425–448. https://doi.org/10.1016/j.trd.2019.02.011

Kiyosugi, K., Connor, C., Sparks, R.S.J., Crosweller, H.S., Brown, S.K., Siebert, L., Wang, T., Takarada, S., 2015. How many explosive eruptions are missing from the geologic record? Analysis of the quaternary record of large magnitude explosive eruptions in Japan. J Appl. Volcanol. 4, 17. https://doi.org/10.1186/s13617-015-0035-9

Liu, F., Panagiotakos, D., 2022. Real-world data: a brief review of the methods, applications, challenges and opportunities. BMC Med Res Methodol 22, 287. https://doi.org/10.1186/s12874-022-01768-6

Mastin, L., Pavolonis, M., Engwell, S., Clarkson, R., Witham, C., Brock, G., Lisk, I., Guffanti, M., Tupper, A., Schneider, D., Beckett, F., Casadevall, T., Rennie, G., 2022. Progress in protecting air travel from volcanic ash clouds. Bull Volcanol 84, 9. https://doi.org/10.1007/s00445-021-01511-x

McKinley Research, 2023. Ted Stevens Anchorage International Airport. Available at: https://www.alaskatia.org/sites/default/files/2023-03/AEDC%20ANC%20Economic%20Impact%20Report%20-%20FINAL.pdf. (accessed 8.1.25)

Meredith, E.S., Teng, R.X.N., Jenkins, S.F., Hayes, J.L., Biass, S., Handley, H., 2025. Cities near volcanoes: Which cities are most exposed to volcanic hazards? https://doi.org/10.5194/nhess-2024-219

Paredes-Mariño, J., Forte, P., Alois, S., Chan, K.L., Cigala, V., Mueller, S.B., Poret, M., Spanu, A., Tomašek, I., Tournigand, P.-Y., Perugini, D., Kueppers, U., 2022. The lifecycle of volcanic ash: advances and ongoing challenges. Bull Volcanol 84, 51. https://doi.org/10.1007/s00445-022-01557-5

Picquout, A., Lavigne, F., Mei, E.T.W., Grancher, D., Noer, C., Vidal, C.M., Hadmoko, D.S., 2013. Air traffic disturbance due to the 2010 Merapi volcano eruption. Journal of Volcanology and Geothermal Research, Merapi eruption 261, 366–375. https://doi.org/10.1016/j.jvolgeores.2013.04.005

Prata, A.J., Prata, A.T., 2012. Eyjafjallajökull volcanic ash concentrations determined using Spin Enhanced Visible and Infrared Imager measurements. Journal of Geophysical Research: Atmospheres 117. https://doi.org/10.1029/2011JD016800

Prata, F., Rose, B., 2015. Chapter 52 - Volcanic Ash Hazards to Aviation, in: Sigurdsson, H. (Ed.), The Encyclopedia of Volcanoes (Second Edition). Academic Press, Amsterdam, pp. 911–934. https://doi.org/10.1016/B978-0-12-385938-9.00052-3

Reichardt, U., Ulfarsson, G.F., Pétursdóttir, G., 2018. Volcanic ash and aviation: Recommendations to improve preparedness for extreme events. Transportation Research Part A: Policy and Practice 113, 101–113. https://doi.org/10.1016/j.tra.2018.03.024

Scheip, C.M., Wegmann, K.W., 2021. HazMapper: a global open-source natural hazard mapping application in Google Earth Engine. Natural Hazards and Earth System Sciences 21, 1495–1511. https://doi.org/10.5194/nhess-21-1495-2021

Shirato, S., 2013. Volcanic Ash Advisories (Technical Note No. Technical Note No. 380). National Research Institute for Earth Science and Disaster Prevention.

Vagnoni, G., Amante, A., 2023. Sicily airport chaos. Reuters. Available at: https://www.reuters.com/world/europe/catania-airport-sicily-cleared-reopen-main-terminal-2023-08-05/#:~:text=ROME%2C%20Aug%205%20(Reuters),down%20due%20to%20a%20fire. (accessed: 8.6.25)

VOGRIPA, 2025. Volcanic Global Risk Identification and Analysis Project. Available at: https://vogripa.org/index.cfm (accessed 8.1.25)

Watkin, S.C., 2003. The application of AVHRR data for the detection of volcanic ash in a Volcanic Ash Advisory Centre. Meteorological Applications 10, 301–311. https://doi.org/10.1017/S1350482703001063

Wilson, T.M., Stewart, C., Sword-Daniels, V., Leonard, G.S., Johnston, D.M., Cole, J.W., Wardman, J., Wilson, G., Barnard, S.T., 2012. Volcanic ash impacts on critical infrastructure. Physics and Chemistry of the Earth, Parts A/B/C, Volcanic ash: an agent in Earth systems 45–46, 5–23. https://doi.org/10.1016/j.pce.2011.06.006

Witham, C., Kristiansen, N., Gurioli, L., 2024. Improving communication between volcano observatories and volcanic ash advisory centres in Europe—outcomes from a first workshop. Bull Volcanol 86, 91. https://doi.org/10.1007/s00445-024-01775-z

World Bank, 2019. Global Airports [WWW Document]. URL https://datacatalog.worldbank.org/search/dataset/0038117/Global%20Airports?version=2 (accessed 7.18.25).

Zimanowski, B., Wohletz, K., Dellino, P., Büttner, R., 2003. The volcanic ash problem. Journal of Volcanology and Geothermal Research 122, 1–5. https://doi.org/10.1016/S0377-0273(02)00471-7

PART II

Supplement Report

Table of Contents

Tables of Figures

Table of Tables

Introduction

This report complements Part I of the dissertation (Research Paper) and is divided into six sections. Section 1 presents an extended literature review. Section 2 details the materials, methodology, and software used. Section 3 conducts a sensitivity analysis. Section 4 introduces a risk matrix highlighting the airports most at risk. Section 5 presents a case study on the Hunga Tonga eruption. Section 6 outlines the projects future.

1. Extended Literature Review

1.1 Past Experience of Volcanic Ash Advisories

Increased awareness of volcanic ash hazards to aviation was significantly driven by two major inflight encounters in 1982 and 1989. In 1982, Mount Galunggung in West Java erupted, producing a moderate-sized ash cloud that caused major disruptions (Sudradjat and Tilling, 1984). On June 24 and July 13 1982, two separate Boeing 747 aircraft encountered volcanic ash. One, British Airways Flight 9, lost power in all four engines and descended thousands of feet before the crew successfully restarted the engines and landed safely. A second plane also experienced the failure of three engines. Despite the eruption's moderate scale, the events highlighted the severe risk volcanic ash poses to aviation and triggered a growing international concern (Gourgaud et al., 2000).

This concern was underscored again during the 1989-1990 eruption of the Redoubt Volcano in south-central Alaska (Power et al., 1994). Between December 1989 and February 1990, five commercial jetliners suffered damage after flying through volcanic ash clouds (Miller and Chouet, 1994). The most serious incident occurred on December 15 1989, when KLM Flight 867, a Boeing 747 en route to Anchorage, lost power in all four engines after flying into a dense ash plume. Although the crew managed to restart the engines and land the aircraft safely, the estimated cost of damage exceeded $80 million. While Anchorage International Airport remained operational, most airlines suspended services until coordination and communication among federal agencies improved (Casadevall, 1994).

Following these high-profile encounters and a rapid growth in jet travel, significant global attention was focused on volcanic hazards affecting aviation. The near-disasters of British Airways Flight 9 and KLM Flight 867 prompted the development of formal communication systems and monitoring networks. This led to the establishment of Volcanic Ash Advisory

Centres (VAACs) by the International Civil Aviation Organisation (ICAO) and the World Meteorological Organisation (WMO) in the early 1990s, aimed at safeguarding international air traffic (Fearnley et al., 2018).

1.2 Volcanic Ash Advisory Issuing Process

This new system consists of three core components: observation, advisory, and warning (Figure 1).

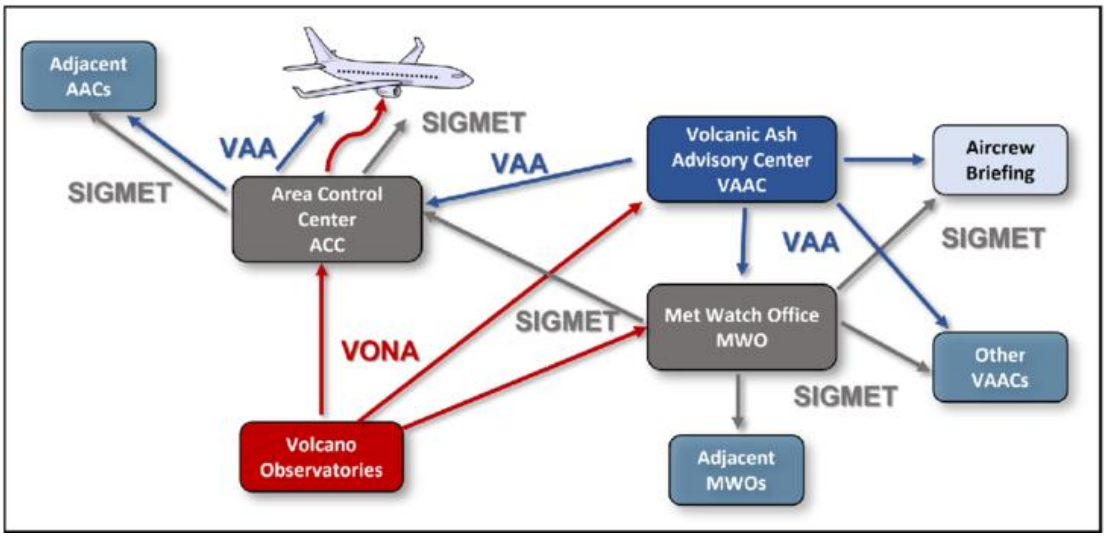

Figure 1: Information Flow between different stakeholders in response to a volcanic eruption (Witham et al., 2024).

1.2.1 Observing

The observing component includes the ground-based monitoring, satellites detection and in-flight reports to detect volcanic eruptions and ash clouds. This information is rapidly shared with Air Traffic Control, Metrological Watch Offices and VAACs (Hufford et al., 2000).

1.2.2 Advisory

This involves the VAACs producing advisory products, such as the Volcanic Ash Advisory (VAA) and its graphical counterpart (VAG) (Figure 2). These advisories provide information on the ash clouds location and activity, the current and forecasted position of ash clouds, plume height, observation sources and the expected timing of the next update (Millington et al.,

2012; Watkin, 2003; Witham et al., 2024). The products are used by Meteorological Watch Offices and Air Traffic Control to support aviation decision-making.

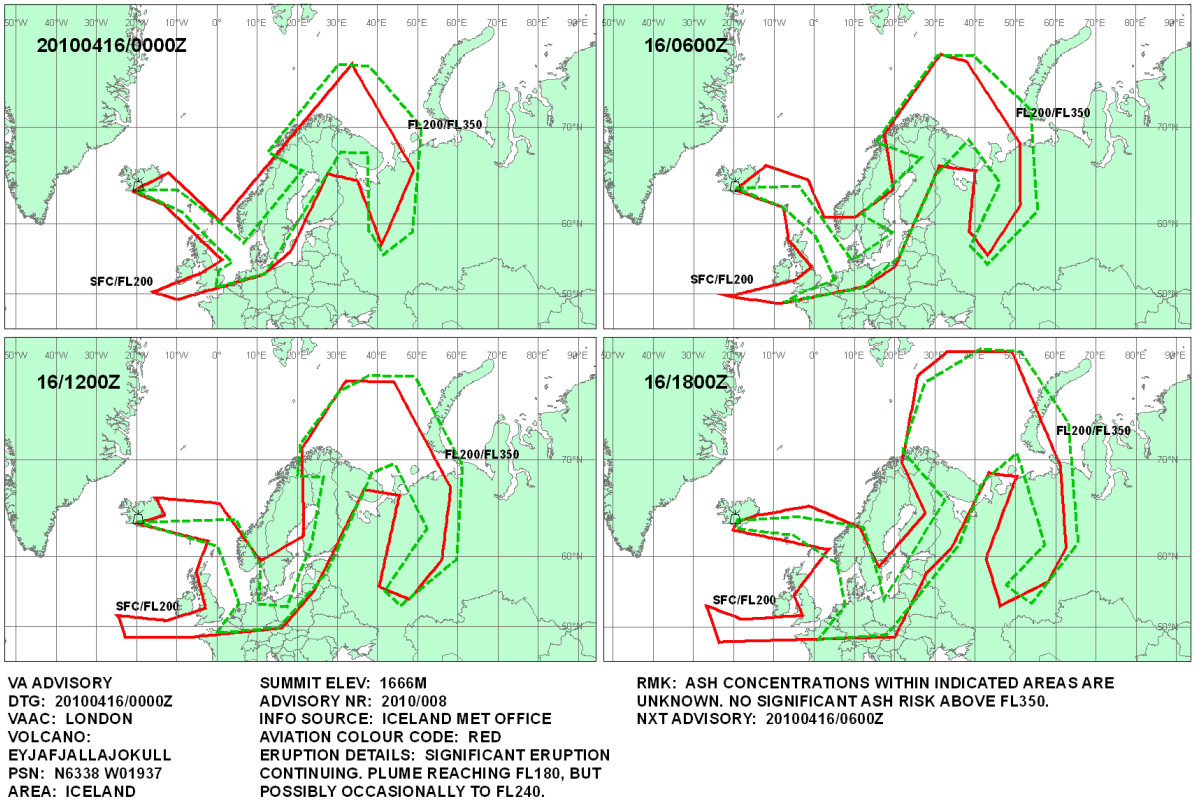

Figure 2: VAA during the 2010 Eyjafjallajökull eruption on the Thursday 15th April 2010 (Met Office, 2010).

To generate these forecasts, observational data is fed into atmospheric dispersion models, which simulate the transport and deposition of ash clouds. These models are driven by numerical weather prediction data from meteorological sources (Witham et al., 2012). For instance, the London VAAC uses the NAME (Numerical Atmospheric-dispersion Modelling Environment) model to simulate ash movement. During the 2010 Eyjafjallajökull eruption, this model was run continuously to predict the ash cloud's trajectory (Millington et al., 2012).

1.2.3 Warning

This component delivers warnings to aircraft and air traffic management through two key message types: SIGMETs, issued by Meteorological Watch Offices to report aviation weather hazards, and NOTAMs, issued by Area Control Centres to communicate changes in airspace status related to volcanic activity (Lechner et al., 2018).

2. Extended Materials and Methodology

2.1 Software

To complete the project efficiently, a range of open-source software tools was selected. These tools were chosen based on their ability to handle large geospatial datasets, integrate with each other and provide flexibility in data analysis and visualisations and reproducibility.

2.1.1 Visual Studio Code

Visual Studio Code was used as the integrated development environment for the project. It provides cross-language support (R, SQL, and Python), Git integration and was compatible with the Universities Linux system. This made it well-suited for managing a heterogeneous codebase across local environments, making it an ideal platform for managing the various components of the project.

2.1.2 Python

Python served as the scripting language as it is very suitable for data wrangling, transformation and pre-processing (Gagolewski, 2025). The workflow primarily relied on the (geo)pandas libraries for handling the data, which offers robust data structures and functions for parsing a cleaning data (Bernard, 2016). Alternative libraries such as PyJanitor could have been implemented which offer extensions for pandas for data cleaning, dataset merging and empty row removal (Pappil Kothandapani, 2021). However, as the datasets were in a decent format, these additional libraries were not needed. Pandas was supplemented with geospatial libraries such as Shapely for spatial operations (e.g. union) and Datetime for manipulating temporal indices.

Table 1: Python Libraries

Libraries	Description
pandas	Data manipulation and analysis using tables (DataFrame), including filtering, grouping, and I/O.
geopandas	Adds geospatial support to pandas; enables spatial joins and geometry operations.
shapely	Handles geometric objects (e.g. points); used for buffering, unions and intersections.
matplotlib	Creates static plots and maps; often used to visualise geospatial or tabular data.
pyproj	Transforms coordinate reference.
logging	Tracks code execution and outputs messages for debugging and monitoring.
datetime	Manages date and time data; used for parsing and formatting timestamps.
collections	Provides advanced data containers like defaultdict for efficient data handling.

2.1.3 R

R was used as the primary environment for statistical analysis and graphical visualisation. Its libraries (e.g., ggplot2, dplyr, sf) enabled both spatial and non-spatial data manipulation. Additionally, R's support for data formats like GeoJSON and CSV ensured smooth integration with geospatial datasets. The decision was further supported by evidence that ggplot2 facilitates the creation of clear and interpretable graphics, particularly for complex or faceted data (Myint et al., 2019). While Python's seaborn library also offers analytical tools and integrates well with the broader Pythons data ecosystem (Waskom, 2021), R was chosen due to prior familiarity. Nevertheless, future work may consider adopting Seaborn as it offers better interoperability with other parts of the workflow.

2.1.4 SQL (Duck DB)

SQL was used to create queries that explored relationships between volcanoes and ash clouds. SQL's reusability made it ideal for rerunning simple queries and exporting results to file formats suitable for downstream analysis. DuckDB was chosen as the SQL engine due to its lightweight design and seamless integration with Python. Unlike traditional database systems (Oracle and PostgreSQL), DuckDB allows queries to be executed directly on files such as CSV and GeoJSON, eliminating the need to first import data into a separate database. This

significantly streamlined the workflow and reduced preprocessing time (Raasveldt and Mühleisen, 2019)

2.1.5 Forth

The Forth high-performance computing (HPC) system at the University of Edinburgh was utilised to run computationally intensive tasks. It significantly reduced processing time and allowed other scripts to be worked on concurrently while the main program was running, without the system crashing.

2.1.6 Alternatives

Comprehensive platforms such as Esri's ArcGIS Pro and QGIS offer many of the same analytical capabilities available in Python or R. However, they often lack the same level of customisation and repeatability. In many cases, rerunning processes in these "black box" environments requires manually re-entering or adjusting parameters, which can be time-consuming and error prone. In contrast, scripting languages like Python allow for batch operations, parameter control, and reproducible workflows through version-controlled scripts (Boeing and Arribas-Bel, 2021). Although ArcGIS Pro includes Model Builder, which allows users to chain multiple processes together, it still lacks the flexibility and scalability provided by code-based workflows.

2.1.7 Reproducibility

A key consideration in the selection of software was their ability to support repeatable and adaptable workflows. Given that the input datasets are subject to ongoing updates, it was essential to develop robust and flexible code capable of handling these changes and producing accurate, up-to-date results with minimal manual intervention. By relying on scripting languages and modular code structures, the workflow ensures that analysis steps can be rerun efficiently as new data becomes available. The codebase is available on the M:Drive under the directory '`dissfinal`'. A README file is included to provide guidance on the code structure and usage as this code is intended to be used for future research purpose, or may need to be updated in case of the issue of new advisories or updated airport data. The code is all written in clearly defined functions, within several well commented scripts which can be executed from a single command line passer.

2.2 Materials

2.2.1 Volcanic Ash Advisories

The VAA dataset was provided by the British Geological Survey, offering recent and up-to-date records related to ash dispersion and advisory notices. While the temporal range of this dataset was limited, it was sufficient for conducting a focused analysis of geographic patterns and volcano–ash cloud relationships. Expanding the temporal coverage through a custom database and automated data scraping could have increased the sample size; however, the existing dataset was considered adequate for identifying meaningful global trends.

2.2.2 Holocene Volcanoes

The Smithsonian Institution Global Volcanism Program database was chosen as it is offers comprehensive global coverage, standardised reporting, and frequent use in peer-reviewed geoscience research (Engwell et al., 2021)

2.2.3 Airports

Two datasets were evaluated for representing aviation infrastructure. An initial dataset containing 9,967 global airport locations included many low-traffic or non-commercial airfields (e.g. Duxford Airport, UK), which were not relevant for this study. A second dataset, provided by the World Bank, was selected for its greater relevance. It included 2,175 commercial airports along with passenger volume statistics, allowing for the assessment of potential ash-related disruption. Additionally, monthly data for Fontanarossa was included to provide a breakdown of impacted passengers on a monthly basis

2.2.4 Data integration inconsistency

Combining datasets from different fields often presents significant challenges, including inconsistent data formats, incompatible classification systems, and mismatched naming conventions (Putrama and Martinek, 2024). In this study, joining the VAAs, Holocene volcano records, and airport datasets presented several methodological challenges, as each was developed for different end users from scientists to civil aviation authorities, resulting in varying naming conventions and classifications systems. For example in the volcano dataset, Hunga Tonga is listed as HUNGA TONGA-HUNGA HA'APAI 243040, whereas in the VAAs dataset, the name appears as HUNGA TONGA-HUNGA, with the ID 243040 recorded separately. As a result, the script needed to extract and match numerical identifiers to join the two datasets. Additionally, elevation was recorded in meters in the volcano dataset, while the

VAA dataset reported height in flight levels (FL), representing hundreds of feet, in line with standard aviation practices.

Despite these technical hurdles, the integration of these datasets presents a unique opportunity to combine domain specific knowledge, offering a more holistic understanding of volcanic hazards, their spatial patterns, and their potential impacts on aviation infrastructure. This kind of cross domain data fusion not only supports more informed decision making but also enables new avenues for interdisciplinary research (Y. Zheng, 2015).

2.3 Methodology

This section gives details the extended methodology, providing additional insight into how and why decisions are made at each step. Figure 3 shows the overview of the methodology. See Appendix

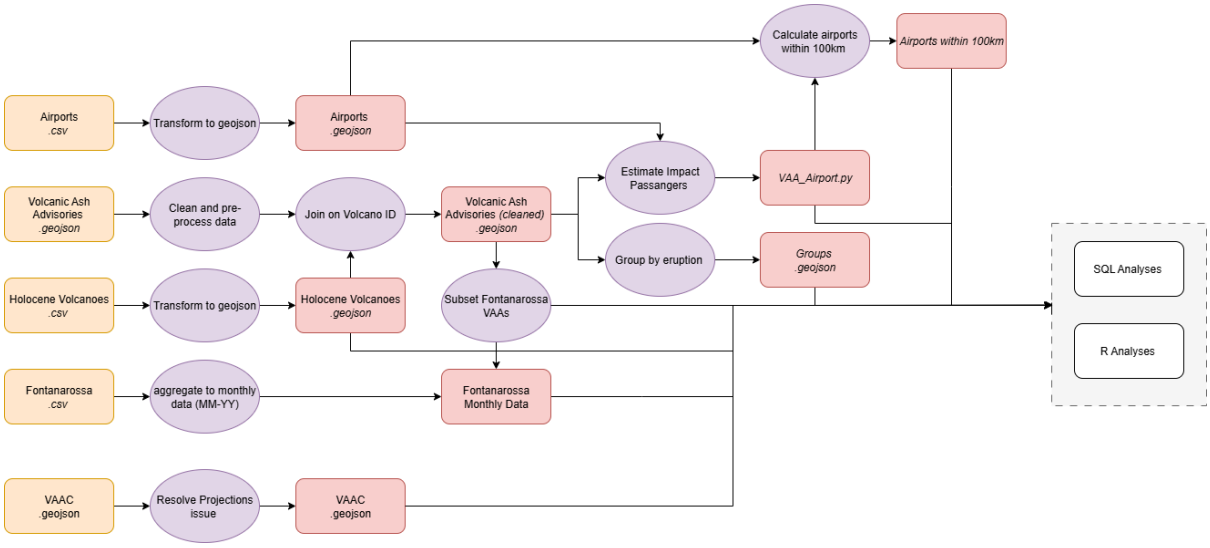

Figure 3: Overview of methodology: (Orange) raw files. (Purple) python scripts. (Red) new data.

2.3.1 Volcanoes and Airports

This script transforms a CSV file into a GeoJSON using pandas so that it could integrated with other datasets as they include a dedicated geometry column, making it suitable for mapping and spatial analysis.

The script loads the data into a pandas DataFrame and uses the `Shapely` library to extract geographic coordinates as point geometries. The coordinate reference system (CRS) is then set to `EPSG:4326` to ensure spatial consistency, as `EPSG:4326` is widely used in geospatial research and is a standard in many scientific publications (Ye et al., 2016).

2.3.2 VAAs.py

The script processes the VAAs GeoJSON provided by the BGS to prepare it for analysis. It begins by applying the `clean date()` function which uses a Boolean mask with `pd.series.str.contains()` to filter out rows with keywords like `"EXERCISE"` or `"TEST"` in the remarks and status fields. This step is performed first to reduce the DataFrame size and minimise computational load. Next, the script corrects geometries that cross the anti-meridian, as Python initially misinterprets these polygons, preventing them from wrapping around the 180° meridian correctly (Figure 4).

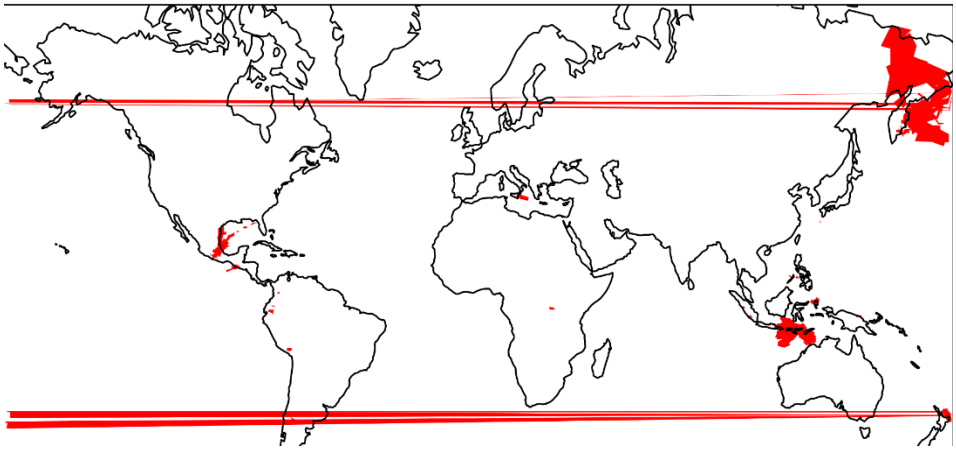

Figure 4: World map displaying VAAs with incorrect geometries, illustrating issues related to date-time formatting and spatial misalignment.

To correct VAAs that crossed the anti-meridian line, the `shiftgeometry()` function was applied. The function iterates over the geometries, adding 360° to longitudes less than 0°, shifting the coordinate system from - 180° to 180° scale to a 0 ° to 360° scale. This resolves geometry distortion, which would otherwise cause some VAAs to appear with exaggerated spatial extents. An alternative solution could involve using a coordinate reference system that handles anti-meridian distortions, such as a Polar Stereographic projection (Figure 5). However, such projections are centred on the poles and result in maps what are difficult to interpret for global scale analysis.

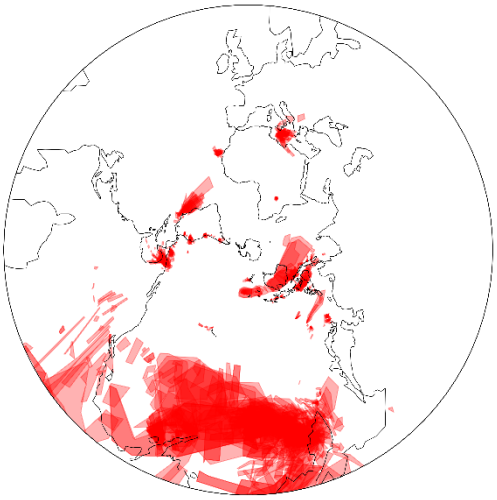

Figure 5: World map displaying VAAs using the Polar Stereographic projection (EPSG:3031).

To understand how plume height influenced the affected area, plume height above vent needed to be calculated, as volcanoes vary significantly in elevation. For instance, Tipas (Argentina) sits at over 6,500 m above sea level, while the Udintsev Transform (Pacific) is located at –5,700 m. Therefore, comparing plume height by flight level (FL) alone, as reported in advisories, does not accurately reflect volcanic explosivity.

To calculate the height in meters, the `calculate_height()` function converted the advisory flight level (FL) to meters, aligning it with the elevation units in the volcano database. The volcano's elevation was then subtracted from the converted FL height to determine the plume height above vent for each advisory.

To calculate the area of the VAAs, the function `calculate_area()` function uses the `PyProj.Geod` class, which accounts for the Earth's curvature by relying on an ellipsoidal Earth model. The function iterates over each geometry in the series and calculates area in square meters, which is then converted to square kilometers (1 m^2 = 1e-6 km^2). This method was chosen over the more common `gdf.area` approach because the dataset is in decimal degrees and spans a 0–360° longitudinal scale to accommodate anti-meridian inconsistencies. Using `gdf.area` would require projecting the data to a metric system like Mercator for accurate area calculations. However, due to inconsistencies and the need to maintain polygons on a 0–360° longitudinal scale, this projection was not feasible.

2.3.3 VAAs and Holocene Volcanoes

To link the VAA data with the Holocene Volcano dataset, a unique identifier is required. The `join_data()` function achieves this by extracting the `Volcano_ID` from the

`Volcano_Name` column using a regular expression with `str.extract()` and then converting it to a float (Table 1).

Table 2: Example of new column to store Volcano ID

Volcano_Name	Volcano_ID
HUNGA TONGA-HUNGA HA'APAI 243040	243040

This approach was preferred over directly matching `Volcano_Name`, as spellings can vary depending on the VAAC issuing the advisory. For example, the Wellington VAAC spells the name as HUNGA TONGA-HUNGA H**A'A**PAI, while Darwin VAAC records it as HUNGA TONGA-HUNGA HA**Â**´APAI. Using `Volcano_ID` (e.g., 243040 in this case) ensures consistent identification and accurate assignment of ash clouds to the correct volcano.

An alternative approach would be to keep the datasets in separate tables and use an SQL query to join them via `Volcano_ID` as the primary key (Figure 6). However, since the datasets are relatively small and did not require multiple joins, the tables were merged to simplify downstream analysis.

```
SELECT *
FROM VAA
JOIN Volcanoes
ON VAA.Volcano_ID = Volcanoes.Volcano_ID;
```

Figure 6: Example of SQL query to join multiple datasets together.

To address the research questions, the analysis was divided into two paths: Path 1 examined volcano–ash cloud characteristics, while Path 2 focused on the impact on aviation.

Path 1: Volcano – Ash Cloud relationship

2.3.4 Grouping

To analyse patterns and trends in VAAs, individual advisories were grouped into eruptive events. An event was defined as a sequence of VAAs in which each advisory was issued within 6.5 hours of the previous one, six hours being the standard interval for reissuance when ash remains in the atmosphere, with an additional 30 minutes to accommodate potential delays.

To group VAAs into eruptive events, a `defaultdict` was used to organise all features by their associated `Volcano_ID`. For each volcano, advisories were sorted chronologically using `dateutil.parser.parse()` on the `observation_dtg` field. The code then iterates through each temporally ordered group, comparing the time difference between consecutive advisories. If the time difference between two observations exceeds six and half hours `(timedelta(hours=6.5))`, a new group is initiated. Otherwise, the event is appended to the current group.

Each resulting cluster of temporally proximate advisories is assigned a unique group identifier in the format `{volcano}_group_{n}`, which is stored in the feature's property dictionary under the key `group_id`. This embedded metadata allows for downstream grouping, filtering, and event-based analysis while maintaining a flat GeoJSON structure.

2.3.1 Duration Calculation

The duration of each group could not be determined by calculating the number of advisories, as some were issued more frequently than the standard six hour interval. Instead for each `group_id`, the `observation_dtg` was extracted and parsed as a datetime object. The duration of each group was then calculated as the time difference between the earliest and latest timestamps. An additional six hours was added to each group's duration to account for the assumed persistence of the final advisory, capturing the full impact of the last reported event.

The computed duration was then assigned to each advisory within the group. Durations were converted from seconds to days, rounded to two decimal places, and stored as a new attribute.

2.3.2 Minimum and Maximum Flight Level Calculation

To calculate the minimum and maximum flight level within each group of advisories, a dictionary `fl_per_group` was created to store lists of `height_above_vent` values grouped by their associated `group_id`. The script iterates through each feature, extracts the `group_id` and `height_above_vent` from the feature's properties, and appends the height to the appropriate group. Once all heights were collected, two dictionaries were constructed: one (`top_fl_min`) which stores the minimum height per group, and (`top_fl_max`) which stores the maximum.

2.3.3 Group area calculation

Once the VAAs were assigned a group id, they were grouped together, to get a singular data entry for each event. This was accomplished using the `groupby ('group_id')` function to group advisories, followed by aggregation using an `agg_dict`. This dictionary returned the first value for each metadata attribute within a group, since attributes other than height and area (e.g., volcano name, location) remained consistent within a group.

As each group could contain multiple advisories with multiple polygons, the total ash cloud area had to be recalculated. This was achieved using the `Shapely union` operation, which merged all polygons within a group into a single geometry representing the total spatial extent of the ash cloud (Figure 5).

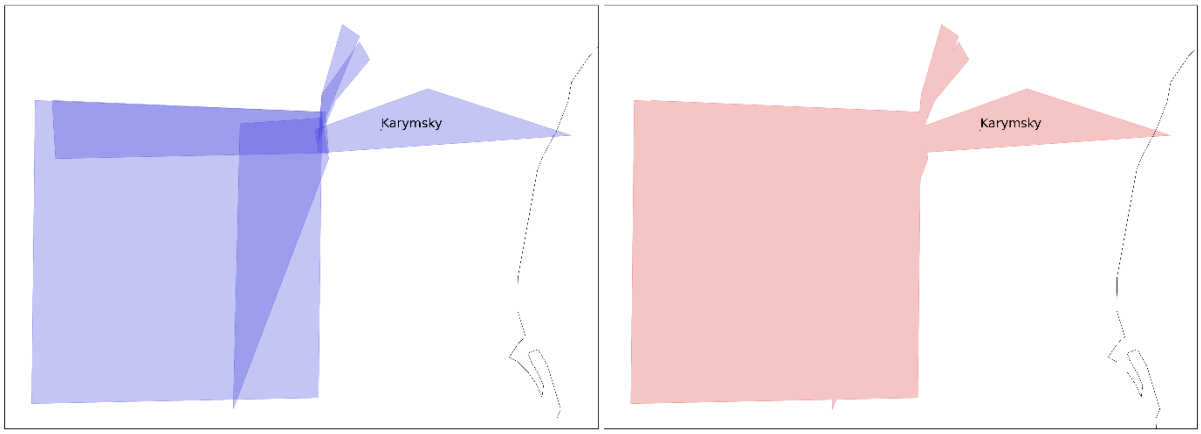

Figure 7: VAAs within a group (left) and after merge (right), demonstrating union tool at Karymsky, Russia (Lechner et al., 2018).

An alternative approach could have involved using a `MultiPolygon`, which allows a GeoJSON feature to contain multiple polygons. However, calculating the area for each individual polygon in this format would risk double counting, as overlapping regions from multiple advisories within the same group could be included more than once.

2.3.4 Airport Analysis (Path 2)

To identify the impact of VAAs on airports, only the VAAs that intersected with an airport were selected for analysis. As if VAAs were grouped using the Path 1 grouping, cases could arise where only a small subset of advisories (e.g. 2 out of 10) intersected with an airport. In such cases, using the full eruption duration would overestimate the actual exposure at the airport and produce misleading results.

To select the overlapping VAAs a spatial join ‘`gpd.sjoin`’ was used with the “`contains`” predicate, which selects only those VAAs that contain airport points. Once the VAAs were reduced to overlapping polygons only, they were grouped using the same approach as described above, with one key exception: airports, rather than volcanoes, were used as the aggregation units. This accounts for the possibility that multiple advisories from different volcanoes may affect the same airport. The `Orig` column, containing the unique IATA airport code was used instead of airport names to reduce the risk of errors from inconsistent capitalisation or typographical variation.

2.3.5 Passenger disruption

To estimate the number of passengers affected during the ash clouds duration at each airport, the passenger traffic data was taken, and using the function `seats_per_day()`, the number of passengers was divided by 365 to produce an estimate of the daily seat capacity at each airport.

To estimate the impact of the ash duration (estimated number of passengers affected per day), ash duration in days was multiplied by the seats/day to provide an estimate into how many travellers were affected during each ash event. Results were rounded to whole numbers, as decimal values did not provide additional insight.

3.3.6 Alternative approach

An alternative approach could be used if higher resolution data, such as monthly or daily passenger traffic per airport were available. This would allow for more accurate estimates of the number of affected travellers. In Python, such an approach could be implemented using time series resampling in pandas (e.g. `resample('D'))` to model passenger flow on a daily scale timescale. However, this would introduce additional complexity including data cleaning, time zone normalisation and interpolation of missing values.

Although this method was not applicable to all airports, monthly passenger data was available for Fontanarossa Airport (CTA), which experienced one of the highest levels of disruption. To focus on this case, the script filtered out all VAAs that did not affect CTA. The monthly passenger dataset was pre-processed by converting the date format to match that of the VAA data. A left join was then used to merge the two datasets on the `YearMonth` field, ensuring that all months with available passenger data were retained. Months without recorded ash events were assigned an ash duration of zero.

2.3.7 Plotting and Graphical Decisions

Several key considerations guided the creation of the figures to ensure clarity and ease of interpretation. First, consistent colour schemes were applied across all graphs; each rock type or VAAC was assigned a fixed colour to facilitate comparison. Second, logarithmic scales were used on the x-axis for most plots to accommodate the wide range of ash duration values, especially given the unusually large eruption from Hunga Tonga, which introduced significant disparity in the data.

3. Sensitivity Analysis

Assessments of aviation disruption caused by volcanic ash are highly sensitive to assumptions about the spatial extent of ash clouds, as satellite data may not accurately capture their full dispersion (Mastin et al., 2022). This sensitivity analysis evaluates how increasing the size of VAAs, to account for uncertainties in ash dispersion observations, influences estimate of disruption (Tortorelli and Michaleris, 1994).

3.1 Method

To account for uncertainties in ash cloud boundaries, buffer zones of 1 km, 5 km, and 25 km were applied around each cleaned VAA. These expanded advisories were then processed through the airport analysis workflow to evaluate how changes in advisory size affect the number of airports classified as at risk. (Step:2.3.4).

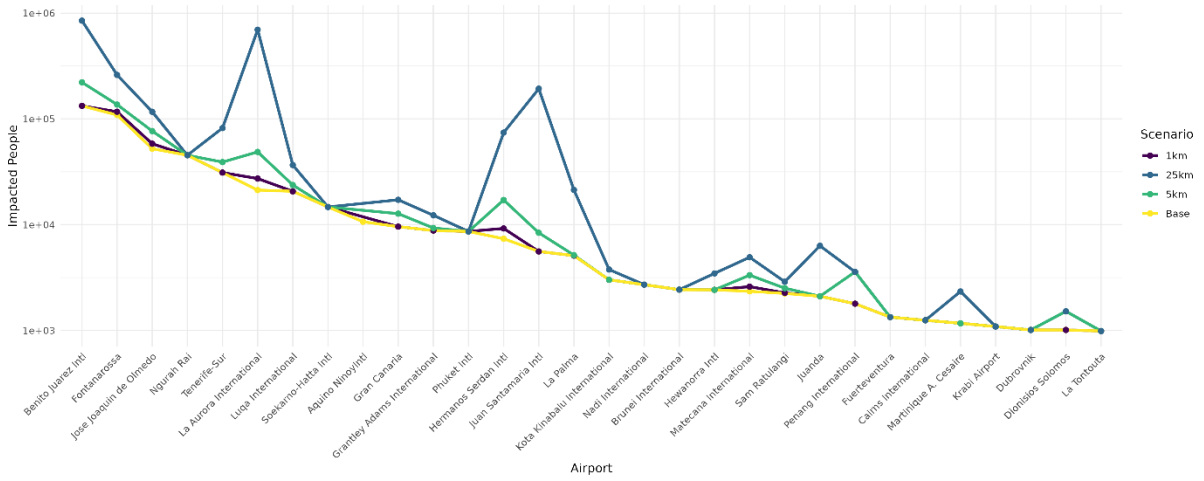

Figure 8: Top 30 airports with the most disruption. Each line represents an incremented increased buffer.

For most airports, the number of impacted passengers increases gradually with buffer distances of 1,000 m and 5,000 m. However, at a 25,000 m buffer, several airports, including La Aurora International, Juan Santamaría International, and Hermanos Serdán International experience a marked increase in disruption.

3.2 Regression Analysis

Regression analysis was used to conduct a sensitivity analysis of how buffer distance influences airport passenger volumes. By treating buffer distance as the predictor and passenger throughput as the response variable, this approach quantifies the extent to which spatial assumptions affect estimated operational impact.

Linear regression analysis was conducted to examine the relationship between base advisory and impact estimates at varying buffer sizes (1km, 5km and 25km). The models for smaller buffer sizes (1 km and 5 km) demonstrated exceptionally strong correlations with the baseline, explaining over 97% and 99% of the variance respectively ($R^2 = 0.9711$ and 0.9976), with highly significant p-values ($< 2 \times 10^{-16}$). In contrast, the largest buffer size (25 km) showed a significantly weaker association ($R^2 = 0.5704$), despite a statistically significant positive slope ($p < 2 \times 10^{-16}$). These findings indicate that small spatial uncertainties do not substantially alter estimates of the number of impacted people; however, beyond a threshold, uncertainties begin to meaningfully affect impact assessment.

While global sensitivity techniques like the Fourier Amplitude Sensitivity Test also offer comprehensive insights, their added complexity and computational cost are unwarranted in this case, where the analysis focuses on a single input variable with a well-defined effect (Christopher Frey and Patil, 2002).

3.3 Case Study: Juan Santamaría International Airport, Costa Rica

Juan Santamaría International Airport ranks as the 14th most disrupted airport under baseline conditions. When a 25 km buffer is applied to account for uncertainty in VAA modelling, it rises to the 3rd most impacted airport. This substantial increase is attributed to the high concentration of VAAs in the surrounding airspace (Figure 9).

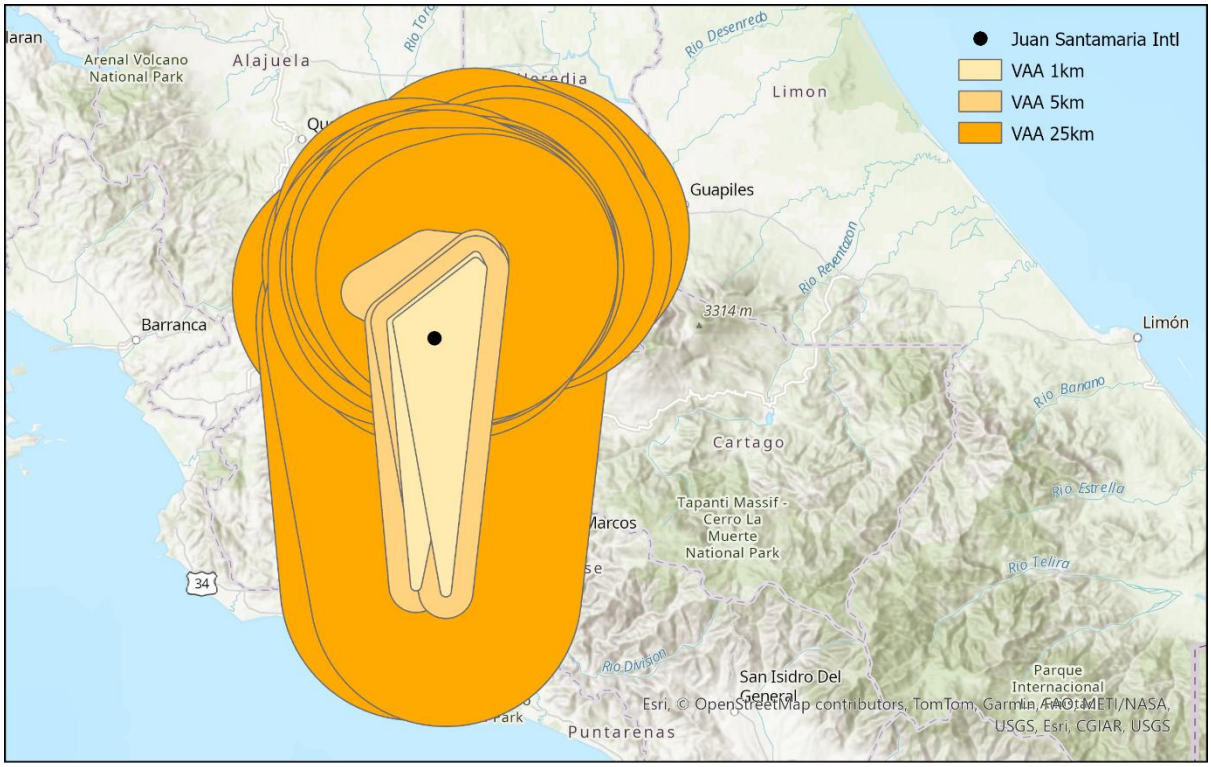

Figure 9: Juan Santamaria Intl airport and its buffers (Esri, 2025).

With a buffer of 1 km, only two additional VAAs affect Juan Santamaría International Airport. This number increases to three with a 5 km buffer and rises sharply to 43 with a 25 km buffer. These results underscore how incorporating uncertainty in advisory boundaries can substantially alter the estimated impact on airports that initially appear only marginally affected. In addition, although this study does not directly analyse flight paths, increasing the buffer serves as a proxy for potential disruption, as airspace around an airport is likely to be affected.

4. Airports Most at Risk

The analysis could be further refined by incorporating the operational vulnerability of airports based on their geographical context. Airports located in isolated regions, such as Ngurah Rai in Indonesia, are more susceptible to disruption due to limited options for nearby diversions. In contrast, airports situated in densely interconnected urban areas benefit from greater routing flexibility, which reduces their relative vulnerability (Verma et al., 2014). Figure 10 illustrates the distribution of airports with alternative facilities located within a 100 km radius, highlighting spatial disparities in operational resilience.

4.1 Method

To assess the availability of nearby alternative airports, each affected airport was buffered by 100 km and a spatial join was conducted with the full airport dataset to identify how many airports fell within each buffer zone (Figure 10). To avoid counting the airport initiating the buffer, one was subtracted from the resulting count. This adjustment ensures that airports are not considered as alternatives to themselves.

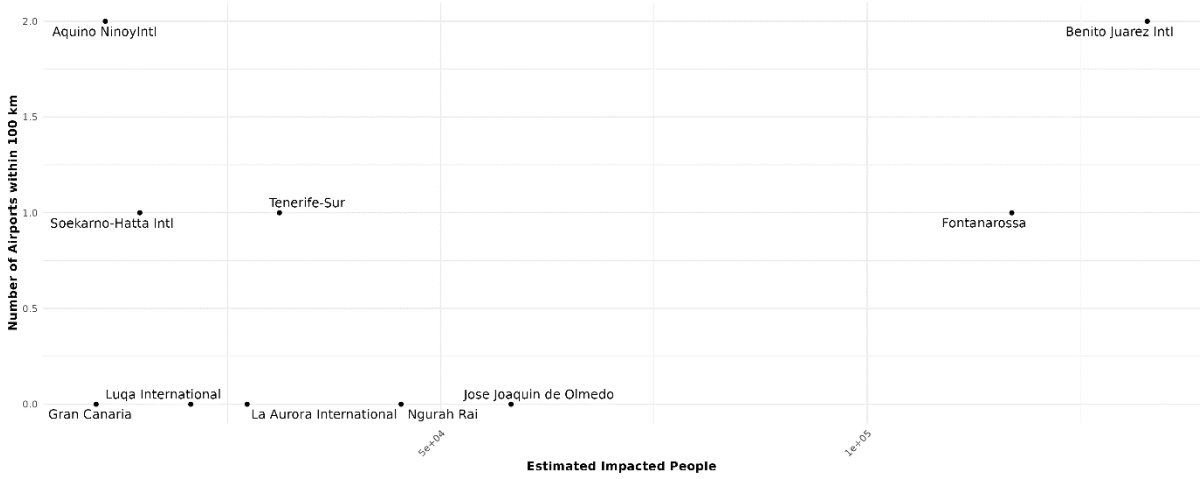

Figure 10: Airports with the highest disruption and number of alternative airports within a 100 km radius.

While the two most impacted airports, Fontanarossa and Benito Juarez Intl Airport have relatively good rerouting options, the uneven impact of airport disruptions across island regions underscores disparities in infrastructure resilience. More developed areas, such as Sicily, benefit from extensive aviation networks and regional connectivity. In contrast, Ngurah Rai, the primary gateway to Bali, is significantly more vulnerable, with only one major alternative located on a separate island. Similarly, José Joaquín de Olmedo is one of four major airports in Ecuador, of which two can accommodate large international aircraft (Logistics

Cluster, 2025). Crucially, the presence of an alternative airport does not ensure sufficient capacity to absorb diverted traffic. Many transcontinental aircraft require long runways and specialised facilities that regional airports may lack (Narcizo et al., 2020). As a result, the closure of a single hub can place considerable strain on surrounding airports, compounding overall disruption. Moreover, Benito Juárez International has two alternative airports located 65 km and 80 km away, respectively. However, its nearest alternative is often affected by the same ash event. This is a common occurrence, as volcanic ash clouds frequently extend far enough to disrupt multiple airports within the same region.

4.2 Limitations

While the sensitivity analysis identifies airports at higher risk due to limited rerouting alternatives, it does not account for the practical aspects of ground transport between airports. For example, the closest airport to Fontanarossa is Tito Minniti Airport, located on the southern coast of mainland Italy. However, despite its proximity in straight-line distance, it may be less accessible than an airport located further away on the island of Sicily, which can be reached more easily by road. For future work, the assessment of alternative airports should incorporate two key criteria: the absence of ash contamination and realistic ground accessibility. Rather than relying solely on straight-line distances, network analysis could be employed to calculate real-world travel times and distances to the next closest suitable airports (Fischer, 2004).

4.3 Proposed Development of a future tool to assess which airports are most at risk

4.3.1 What is a risk matrix?

To identify airports most susceptible to disruption, a risk matrix was proposed. Risk matrices provide a structured and quantitative framework for assessing and prioritising hazards (Datta and Mukherjee, 2001). By evaluating the probability, severity and exposure associated with each risk, they help identify the areas of highest concern (Chartres et al., 2019). For example, a risk matrix was effectively employed during the 2013 Salzach flood in Austria, enabling authorities to prioritise resources and implement targeted mitigation strategies in advance of the event (Spiekermann et al., 2015).

4.3.2 Volcanic ash and risk matrices

In this study, the risk matrix could identify vulnerable airports by accounting for both direct factors and secondary factors, such as passenger volume and the availability of alternative

airports for rerouting. This information could enable stakeholders to prioritise high-risk airports and develop contingency plans, including establishing temporary inter-airport connections and preparing secondary sites for increased passenger loads in the event of closures (Datta and Mukherjee, 2001).

Assigning a risk-based management scale for airports would require a two-step approach, as there are multiple influencing factors extended beyond the scope of traditional methods such as Cox, (2008). Before calculating risk scores, the input data would have to be standardised using Z-score normalisation to address high variability among variables. This technique transforms data to a common scale with a mean of zero and a standard deviation of one, preventing variables with larger ranges from disproportionately influencing the results (Gorricha and Lobo, 2012).

$$Z = \frac{X - \mu}{\sigma}$$

Standardisation Equation: X represents the original variable, μ is the mean, σ is the standard deviation and Z is the standardised variable.

Once the variables were normalised, the World Bank's equation was adapted to calculate a composite impact factor, which was then integrated them into the risk matrix (World Bank, 2014). Risk at each airport was computed by multiplying passenger volume (exposure) by distance to suitable alternative airports (vulnerability).

$$Impact = Exposure\ x\ Vulnerbility$$

With standardised risk scores for each airport, values would need to be classified into Low, Medium, and High Impact. A risk matrix could then be constructed with two axes representing probability and level of risk, with probability estimates derived from historical VAAs data. These results then help identify which airports require the most comprehensive contingency planning.

Table 3: Risk Matrix

		Risk		
Probability		Low Impact	Medium Impact	High Impact
	Low Risk of Closure	LOW (1)	LOW (2)	MEDIUM (3)
	Medium Risk of Closure	LOW (2)	MEDIUM (4)	HIGH (6)
	High Risk of Closure	MEDIUM (3)	HIGH (6)	HIGH (9)

5. The 2022 Hunga Tonga-Hunga Ha’apai eruption

5.1 Background

On January 15 2022, Hunga Tonga-Hunga Ha’apai (HTHH), a submarine volcanic located between the uninhabited islands of Hunga Tonga and Hunga Ha'apai, erupted and generated one of the largest ash clouds of the past century (Amores et al., 2022). The eruption generated ash plumes that reached altitudes of 58 km. Among its ten eruptive events, the two largest covered areas of 16,462,486 km² and 13,370,547 km², respectively together exceeding the combined coverage of the next 30 largest eruptions. Moreover, the average area affected by a typical eruption is approximately 8,000 km², making HTHH's largest event over 2,000 times larger.

5.2 Impact of Aviation

Although this was the largest volcanic event during the study period, its impact on aviation was limited compared to eruptions such as those from Mount Etna. This is primarily due to three factors. First, the volcano is located in the South Pacific, far from major airports. Second, despite its intensity, the eruption was brief, with significant activity limited between

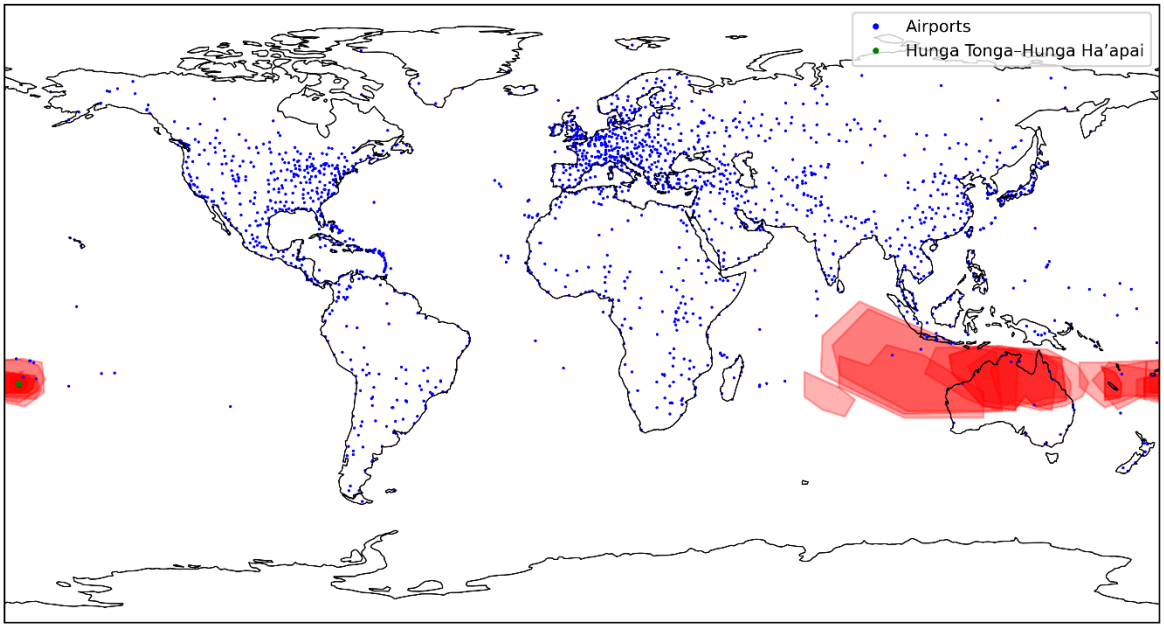

Figure 11: World map with Hunga Tonga Eruption and world airports.

December 20 and January 20. Third, the findings presented in this study are influenced by the recovering effects of the COVID-19 pandemic, during which global air traffic was significantly reduced (Dube, 2023).

However, the eruption of HTHH generated powerful atmospheric waves, including gravity waves and acoustic waves which propagated globally and caused significant atmospheric fluctuations (Wright et al., 2022). These disturbances led to sudden and abnormal changes in atmospheric pressure, posing serious risks to aviation navigation systems that rely heavily on accurate air pressure measurements to determine aircraft altitude (Sun et al., 2024).

In aviation, altimeters calculate an aircraft's altitude based on surrounding air pressure. While sudden pressure changes caused by volcanic-induced atmospheric waves can lead to incorrect altitude readings. For example, if atmospheric pressure suddenly drops, the altimeter may indicate a higher altitude than the actual position, causing the aircraft to overshoot its landing touching down farther than planned. Conversely, a sudden rise in pressure may show a lower altitude, leading to an undershoot, where the aircraft lands short of the intended touchdown zone (Ismanto et al., 2023).

While most of this study examines how volcanic ash affects aviation by analysing its impact on airports, this case study highlights that major eruptions can influence aviation in ways other than direct ash cloud exposure. Because such large-scale events are uncommon, it is more effective to focus research on regions where ash-related disruptions are most frequent and severe, as demonstrated in this study.

5.3 Possibility of greater impact

Had a similar event taken place near a major population area, it could have caused severe social and societal damage. To assess the potential impact of such an eruption in a more populated region, the Hunga Tonga–Hunga Ha'apai event was modelled as if it had occurred over mainland Europe. (Figure 12).

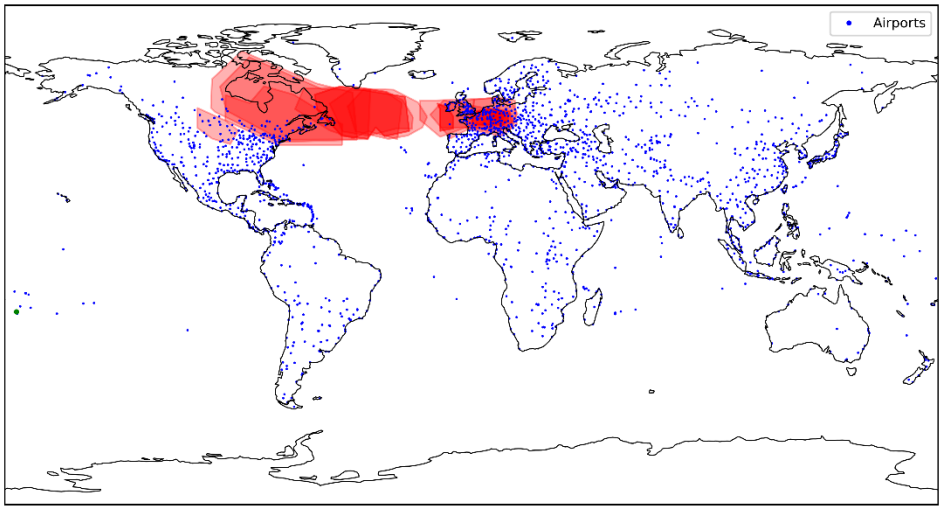

Figure 12: New projection transformation of HTTH on a world map.

The results showed 35 intersections with airports and an estimated 418,158 passengers potentially affected. This underscores how a rare eruption of this magnitude could have a severe impact if it occurred in a more densely populated region with numerous and frequently used transport links.

6. Future of the Project

Despite advancements in the integration of various data sources and technologies for VAAs, significant challenges persist in ensuring that this information is both accessible and usable by a wider range of stakeholders. Lechner et al. (2018) advocate for the consolidation of data from multiple VAACs to establish a coordinated alert system, emphasising the importance of real-time hazard information delivery to aircraft cockpits. Capponi et al. (2022) developed a tool aimed at reducing flight disruptions by merging satellite observations with volcanic ash dispersion and transport modelling. Meanwhile, Witham et al., (2024) highlight the necessity of enhancing communication pathways between VAACs and Volcanic Observatories, alongside implementing harmonized protocols for the dissemination of official advisories.

While a number of tools have been developed to support volcanic ash advisory systems, they predominantly focus on operational stakeholders such as aircrews and air traffic controllers, offering limited capabilities for cross-comparison of VAAs on a global scale or across temporal dimensions. This limits effective interpretation and weakens hazard communication and risk management strategies. Both Scaini et al. (2014) and Pallister et al. (2019) advocate for the creation of a globally accessible hazard map, serving as a gateway to a comprehensive digital platform that consolidates both real-time and historical VAA data for a broader user base.

My research demonstrates that it is feasible to compile all existing VAA information and relevant airport data into a single data source. By using API keys, the system could be regularly updated, ensuring real time accuracy. Additionally, user-driven analytical tools could be incorporated, allowing users to explore patterns, compare events and make data-informed decisions. This framework provides a foundation for future developments aimed at closing existing communication and accessibility gaps in volcanic hazard monitoring.

Bibliography

Amores, A., Monserrat, S., Marcos, M., Argüeso, D., Villalonga, J., Jordà, G., Gomis, D., 2022. Numerical Simulation of Atmospheric Lamb Waves Generated by the 2022 Hunga-Tonga Volcanic Eruption. Geophysical Research Letters 49, e2022GL098240. https://doi.org/10.1029/2022GL098240

Bernard, J., 2016. Python Data Analysis with pandas, in: Bernard, J. (Ed.), Python Recipes Handbook: A Problem-Solution Approach. Apress, Berkeley, CA, pp. 37–48. https://doi.org/10.1007/978-1-4842-0241-8_5

Boeing, G., Arribas-Bel, D., 2021. GIS and Computational Notebooks. https://doi.org/10.48550/arXiv.2101.00351

Capponi, A., Harvey, N.J., Dacre, H.F., Beven, K., Saint, C., Wells, C., James, M.R., 2022. Refining an ensemble of volcanic ash forecasts using satellite retrievals: Raikoke 2019. Atmospheric Chemistry and Physics 22, 6115–6134. https://doi.org/10.5194/acp-22-6115-2022

Casadevall, T.J., 1994. The 1989–1990 eruption of Redoubt Volcano, Alaska: impacts on aircraft operations. Journal of Volcanology and Geothermal Research, The 1989-1990 Eruptions of Redoubt Volcano, Alaska 62, 301–316. https://doi.org/10.1016/0377-0273(94)90038-8

Chartres, N., Bero, L.A., Norris, S.L., 2019. A review of methods used for hazard identification and risk assessment of environmental hazards. Environment International 123, 231–239. https://doi.org/10.1016/j.envint.2018.11.060

Christopher Frey, H., Patil, S.R., 2002. Identification and Review of Sensitivity Analysis Methods. Risk Analysis 22, 553–578. https://doi.org/10.1111/0272-4332.00039

Cox, L., 2008. What's Wrong with Risk Matrices? Risk Analysis 28, 497–512. https://doi.org/10.1111/j.1539-6924.2008.01030.x

Datta, S., Mukherjee, S.K., 2001. Developing a Risk Management Matrix for Effective Project Planning—An Empirical Study. Project Management Journal 32, 45–57. https://doi.org/10.1177/875697280103200206

Dube, K., 2023. Emerging from the COVID-19 Pandemic: Aviation Recovery, Challenges and Opportunities. Aerospace 10, 19. https://doi.org/10.3390/aerospace10010019

Engwell, S., Mastin, L., Tupper, A., Kibler, J., Acethorp, P., Lord, G., Filgueira, R., 2021. Near-real-time volcanic cloud monitoring: insights into global explosive volcanic eruptive activity through analysis of Volcanic Ash Advisories. Bull Volcanol 83, 9. https://doi.org/10.1007/s00445-020-01419-y

Esri. *(2025)*. World Topographic Ma**p** [basemap]. *World Topographic Map*. ArcGIS Online. Available at: https://www.arcgis.com/home/item.html?id=30e5fe3149c34df1ba922e6f5bbf808f (accessed: 8.1.25)

Fearnley, C., Winson, A.E.G., Pallister, J., Tilling, R., 2018. Volcano Crisis Communication: Challenges and Solutions in the 21st Century, in: Fearnley, C.J., Bird, D.K., Haynes, K., McGuire, W.J., Jolly, G. (Eds.), Observing the Volcano World: Volcano Crisis Communication. Springer International Publishing, Cham, pp. 3–21. https://doi.org/10.1007/11157_2017_28

Fischer, M.M., 2004. GIS and Network Analysis, in: Hensher, D.A., Button, K.J., Haynes, K.E., Stopher, P.R. (Eds.), Handbook of Transport Geography and Spatial Systems. Emerald Group Publishing Limited, p. 0. https://doi.org/10.1108/9781615832538-022

Gorricha, J., Lobo, V., 2012. Improvements on the visualization of clusters in geo-referenced data using Self-Organizing Maps. Computers & Geosciences 43, 177–186. https://doi.org/10.1016/j.cageo.2011.10.008

Gourgaud, A., Thouret, J.-C., Bourdier, J.-L., 2000. Stratigraphy and textural characteristics of the 1982–83 tephra of Galunggung volcano (Indonesia): implications for volcanic hazards. Journal of Volcanology and Geothermal Research 104, 169–186. https://doi.org/10.1016/S0377-0273(00)00205-5

Hufford, G.L., Salinas, L.J., Simpson, J.J., Barske, E.G., Pieri, D.C., 2000. Operational Implications of Airborne Volcanic Ash. Bulletin of the American Meteorological Society 81, 745–755.

Ismanto, H., Hidayati, S., Setia Budi, F., 2023. The effect of the eruption of mount Hunga-Tonga on density altitude, air pressure and flight operations in eastern Indonesian. IOP Conf. Ser.: Earth Environ. Sci. 1233, 012070. https://doi.org/10.1088/1755-1315/1233/1/012070

Lechner, P., Tupper, A., Guffanti, M., Loughlin, S., Casadevall, T., 2018. Volcanic Ash and Aviation—The Challenges of Real-Time, Global Communication of a Natural Hazard, in: Fearnley, C.J., Bird, D.K., Haynes, K., McGuire, W.J., Jolly, G. (Eds.), Observing the Volcano World: Volcano Crisis Communication. Springer International Publishing, Cham, pp. 51–64. https://doi.org/10.1007/11157_2016_49

Logistics Cluster, 2025. Digital Logistics Capacity Assessments [WWW Document]. URL https://www.lca.logcluster.org/ecuador-22-aviation (accessed 8.2.25).

Mastin, L., Pavolonis, M., Engwell, S., Clarkson, R., Witham, C., Brock, G., Lisk, I., Guffanti, M., Tupper, A., Schneider, D., Beckett, F., Casadevall, T., Rennie, G., 2022. Progress in protecting air travel from volcanic ash clouds. Bull Volcanol 84, 9. https://doi.org/10.1007/s00445-021-01511-x

Miller, T.P., Chouet, B.A., 1994. The 1989–1990 eruptions of Redoubt Volcano: an introduction. Journal of Volcanology and Geothermal Research, The 1989-1990 Eruptions of Redoubt Volcano, Alaska 62, 1–10. https://doi.org/10.1016/0377-0273(94)90025-6

Millington, S.C., Saunders, R.W., Francis, P.N., Webster, H.N., 2012. Simulated volcanic ash imagery: A method to compare NAME ash concentration forecasts with SEVIRI imagery for the Eyjafjallajökull eruption in 2010. Journal of Geophysical Research: Atmospheres 117. https://doi.org/10.1029/2011JD016770

Myint, L., Hadavand, A., Jager, L., Leek, J., 2019. Comparison of plotting system outputs in beginner analysts. https://doi.org/10.48550/arXiv.1903.01829

Narcizo, R.R., Alves, C.J., Caetano, M., 2020. The Aircraft Choice Based on the Aircraft Take-Off Runway Length Requirement. J.Aerosp. Technol. Manag. e3120. https://doi.org/10.5028/jatm.v12.1167

Pallister, J., Papale, P., Eichelberger, J., Newhall, C., Mandeville, C., Nakada, S., Marzocchi, W., Loughlin, S., Jolly, G., Ewert, J., Selva, J., 2019. Volcano observatory best practices (VOBP) workshops - a summary of findings and best-practice recommendations. J Appl. Volcanol. 8, 2. https://doi.org/10.1186/s13617-019-0082-8

Pappil Kothandapani, H., 2021. A Benchmarking and Comparative Analysis of Python Libraries for Data Cleaning: Evaluating Accuracy, Processing Efficiency, and Usability Across Diverse Datasets 5, 16–33.

Power, J.A., Lahr, J.C., Page, R.A., Chouet, B.A., Stephens, C.D., Harlow, D.H., Murray, T.L., Davies, J.N., 1994. Seismic evolution of the 1989–1990 eruption sequence of Redoubt Volcano, Alaska. Journal of Volcanology and Geothermal Research, The 1989-1990 Eruptions of Redoubt Volcano, Alaska 62, 69–94. https://doi.org/10.1016/0377-0273(94)90029-9

Putrama, I.M., Martinek, P., 2024. Heterogeneous data integration: Challenges and opportunities. Data Brief 56, 110853. https://doi.org/10.1016/j.dib.2024.110853

Raasveldt, M., Mühleisen, H., 2019. DuckDB: an Embeddable Analytical Database, in: Proceedings of the 2019 International Conference on Management of Data. Presented at the SIGMOD/PODS '19: International Conference on Management of Data, ACM, Amsterdam Netherlands, pp. 1981–1984. https://doi.org/10.1145/3299869.3320212

Scaini, C., Folch, A., Bolić, T., Castelli, L., 2014. A GIS-based tool to support air traffic management during explosive volcanic eruptions. Transportation Research Part C: Emerging Technologies 49, 19–31. https://doi.org/10.1016/j.trc.2014.09.020

Spiekermann, R., Kienberger, S., Norton, J., Briones, F., Weichselgartner, J., 2015. The Disaster-Knowledge Matrix – Reframing and evaluating the knowledge challenges in disaster risk reduction. International Journal of Disaster Risk Reduction 13, 96–108. https://doi.org/10.1016/j.ijdrr.2015.05.002

Sudradjat, A., Tilling, R., 1984. Volcanic Hazards in Indonesia: The 1982-83 Eruption of Galunggung. International Union of Geological Sciences 7, 13–19. https://doi.org/10.18814/epiiugs/1984/v7i2/004

Esri. (2025). World Topographic Map [basemap]. World Topographic Map. ArcGIS Online. Available at: https://www.arcgis.com/home/item.html?id=30e5fe3149c34df1ba922e6f5bbf808f (Accessed: 2025).

Sun, Q., Lu, T., Li, D., Xu, J., 2024. The Impact of the Hunga Tonga–Hunga Ha'apai Volcanic Eruption on the Stratospheric Environment. Atmosphere 15, 483. https://doi.org/10.3390/atmos15040483

Tortorelli, D.A., Michaleris, P., 1994. Design sensitivity analysis: Overview and review. Inverse Problems in Engineering 1, 71–105. https://doi.org/10.1080/174159794088027573

Verma, T., Araújo, N.A.M., Herrmann, H.J., 2014. Revealing the structure of the world airline network. https://doi.org/10.48550/arXiv.1404.1368

Waskom, M.L., 2021. seaborn: statistical data visualization. Journal of Open Source Software 6, 3021. https://doi.org/10.21105/joss.03021

Watkin, S.C., 2003. The application of AVHRR data for the detection of volcanic ash in a Volcanic Ash Advisory Centre. Meteorological Applications 10, 301–311. https://doi.org/10.1017/S1350482703001063

Witham, C., Kristiansen, N., Gurioli, L., 2024. Improving communication between volcano observatories and volcanic ash advisory centres in Europe—outcomes from a first workshop. Bull Volcanol 86, 91. https://doi.org/10.1007/s00445-024-01775-z

Witham, C., Webster, H., Hort, M., Jones, A., Thomson, D., 2012. Modelling concentrations of volcanic ash encountered by aircraft in past eruptions. Atmospheric Environment, Volcanic ash over Europe during the eruption of Eyjafjallajöekull on Iceland, April-May 2010 48, 219–229. https://doi.org/10.1016/j.atmosenv.2011.06.073

World Bank, 2014. *Understanding risk in an evolving world: Emerging best practices in natural disaster risk assessment.* [online] Washington, DC: World Bank. Available at: https://documents1.worldbank.org/curated/en/907841468181459620/pdf/921660WP0Box380in0an0Evolving0World.pdf (accessed: 8.5.25)

Wright, C.J., Hindley, N.P., Alexander, M.J., Barlow, M., Hoffmann, L., Mitchell, C.N., Prata, F., Bouillon, M., Carstens, J., Clerbaux, C., Osprey, S.M., Powell, N., Randall, C.E., Yue, J., 2022. Surface-to-space atmospheric waves from Hunga Tonga–Hunga Ha'apai eruption. Nature 609, 741–746. https://doi.org/10.1038/s41586-022-05012-5

Y. Zheng, 2015. Methodologies for Cross-Domain Data Fusion: An Overview. IEEE Transactions on Big Data 1, 16–34. https://doi.org/10.1109/TBDATA.2015.2465959

Ye, S., Yan, T., Yue, Y., Lin, W., Li, L., Yao, X., Mu, Q., Li, Y., Zhu, D., 2016. Developing a reversible rapid coordinate transformation model for the cylindrical projection. Computers & Geosciences 89, 44–56. https://doi.org/10.1016/j.cageo.2016.01.007

Appendix

1. Data Sources

1.1 Data Location

Data is available on m:s2758252/dissfinal – with the omission of the VAAs data which is owned by the BGS. Scripts are also available at freddiegi02 on GitHub (https://github.com/freddiegi02/Diss.git)

1.2 File Structure

Name	Description	Supplier	Format
Datasets			
Airports	Global Airports with pass no	World Bank	csv
Fontanarossa	Monthly pass no	Aeroporti	Csv
vaa	VAAs (2020 – 2025)	BGS	Geojson
Holecene_Volcs	Holocene Volcanoes	Smithsonian	csv
Scripts			
Airport_Buffer	Airport Buffer Plotting		.py
Airport_Transform	Transform Airports		.py
Fontanarossa_study	Calc Impact each Month		.py
Group	Groups VAAs to Volcanic Event		.py
Impact_Pass	Calcs Impact People		.py
Transform_HTTH	Translates to over Europe		.py
Heatmap_Airports	Heatmap of VAAs and Airports		.py
Heatmaps_Volcs	Heatmaps of VAAs and Volcs		.py
merge_buffer	Merges the buffers		.py
Plot_Map	Plots VAAs		.py
plot_union	Plots Union Tool		.py
Airports_Pass	Airport Affected Graph		,r
Airports_Within	Airports close to each other		.r
Area_Height	Area v Height Graphs		.r
Area_Height_Graphs	Area and Height Graphs		.r
Area_Time	VAAs v Volcanic Event		.r
Ash_Duration	Ash Duration Impact		.r
Fontanarossa	Monthly Data at Fontanarossa		.r
Most_Affected_Airport	Most Affected Airports Graph		.r
Sensitivity	Sensitivity Analysis		.r

2. Datasets

2.1 Raw Data

Contains the data in their raw format

2.1.1 Volcano

Volcano Number	Volcano Name	Country	Volcano Region	Volcano Province	Volcano Landform
Activity Evidence	Last Know Eruption	Latitude	Longitude	Elevation	Tectonic Setting
Primary Volcano Type	Dominant Rock Type				

2.1.2 Airport Data

Orig	Airport Name	TotalSeats	Latitude	Longitude

2.1.3 VAAs

File	vaac	volcano	dtg	speed
status	aviation_colour_code	observed_cloud_extent	observed_cloud_max_fl	geometry
remarks	info_source	next_advisory	forecast_cloud_extent_06hr	header
forecast_cloud_extent_18hr	area	position	observation_dtg	base_fl
forecast_cloud_extent_12hr	eruption_details	summit_elevation	layer_id	dtg_date
top_fl	heading	advisory_number		

2.1.4 VAAC

vaac	geometry

2.2 Secondary Data

Contains the data once analysed and used for plotting and SQL queries

2.2.1 VAAs Processed

Volcano Number	'Volcano Name	'Country	Primary Volcano Type	Elevation (m)	Dominant Rock Type
File	vaac	dtg	observation_dt	dtg_date'	layer_id'
base_fl	top_fl	true_height	area_combined	geometry	

2.2.2 VAA Airport

Rock Type	Elevation (m)	Orig	Primary Volcano Type	TotalSeats	Impact_People
Volcano	Volcano Number	area_combined	base_fl	dtg	dtg_date
File	index_right	layer_id	observation_dtg	top_fl	true_height
vaac	volcano	group_id	ash_duration_day	Seats_Day	

2.2.3 VAAs Groups

group_id	Country	Dominant Rock Type	Elevation (m)	Primary Volcano Type	Volcano Name
Volcano Number	area_combined	base_fl	dtg	dtg_date	file
layer_id	observation_dtg	top_fl	true_height	vaac	volcano
ash_duration_day	top_fl_min	top_fl_max	geometry		

2.2.4 Fontanarossa

pass_nos	YearMonth	ash_duration_day

3. Code Example

3.1 VAA processing script

```
import geopandas as gpd
from shapely.geometry import mapping, shape
import shapely
from pyproj import Geod

def clean_data(gdf):
    return gdf[
        ~gdf['remarks'].str.contains("EXERCISE|TEST", na=False, case=False) &
        ~gdf['status'].str.contains("EXER", na=False, case=False)
    ]
def shift_geometry(geom):
    if geom is None:
        return None

    def shift_lon(lon):
        return lon + 360 if lon < 0 else lon

    def shift_coords(coords):
        return [(shift_lon(x), y) for x, y in coords]

    if geom.type == 'Polygon':
        return shapely.geometry.Polygon(
            shift_coords(geom.exterior.coords),
            [shift_coords(ring.coords) for ring in geom.interiors]
        )
    else:
        return geom

def join_data(vaa, volcano):
    vaa['volcano_number'] = vaa['volcano'].str.extract(r'(\d+)$').astype(float)
    volcano['volcano_number'] = volcano['Volcano Number']

    joined_gdf = volcano.merge(vaa, on='volcano_number', suffixes=('_vaa', '_volcano'))
    joined_gdf =
joined_gdf.set_geometry('geometry_volcano').drop(columns=['geometry_vaa'])
    return joined_gdf
def calculate_true_height(gdf):
    gdf.loc[:, 'true_height'] = (((gdf['top_fl']) * 100) / 3.281) - gdf['Elevation (m)']
    return gdf

def calculate_area(gdf):
    geod = Geod(ellps="WGS84")
    areas_km2 = []

    for geom in gdf.geometry:
        if geom is None or geom.is_empty:
            areas_km2.append(0)
        elif geom.geom_type == 'Polygon':
            area, _ = geod.geometry_area_perimeter(geom)
            areas_km2.append(abs(area) / 1e6)
        elif geom.geom_type == 'MultiPolygon':
            area_total = sum(abs(geod.geometry_area_perimeter(poly)[0]) for poly in
geom.geoms)
            areas_km2.append(area_total / 1e6)
        else:
            areas_km2.append(0)

    gdf['area_combined'] = [round(a, 2) for a in areas_km2]
    return gdf

def clean_daa(gdf):

    gdf = gdf.drop([ 'Volcanic Region',
       'Volcanic Province', 'Volcano Landform',
       'Activity Evidence', 'Last Known Eruption', 'Latitude', 'Longitude', 'Tectonic
Setting',
       'status', 'aviation_colour_code', 'observed_cloud_extent',
       'observed_cloud_max_fl', 'eruption_details', 'remarks', 'info_source',
       'next_advisory', 'forecast_cloud_extent_06hr',
       'forecast_cloud_extent_12hr', 'forecast_cloud_extent_18hr',
```

```
            'position', 'summit_elevation', 'advisory_number', 'header', "volcano_number",
    "area",
        'heading', 'speed'], axis=1)

        return gdf

    if __name__ == '__main__':
        vaa = gpd.read_file("../../Data/vaa.geojson")
        volcano = gpd.read_file("../../GeoJSON/Holecene_Volcano.geojson")

        vaa = vaa.set_crs("EPSG:4326", allow_override=True)
        volcano = volcano.set_crs("EPSG:4326", allow_override=True)

        vaa_cleaned = clean_data(vaa)
        vaa_cleaned['geometry'] = vaa_cleaned['geometry'].apply(shift_geometry)
        joined_gdf = join_data(vaa_cleaned, volcano)
        joined_gdf = calculate_true_height(joined_gdf)
        joined_gdf = calculate_area(joined_gdf)
        joined_gdf = clean_daa(joined_gdf)
        joined_gdf = joined_gdf.to_crs(epsg=4326)

joined_gdf.to_file("../../GeoJSON/vaa_processed.geojson", driver="GeoJSON")
```